NASA Contractor Report 3550

Developing Flow in S-Shaped Ducts

I - Square Cross-Section Duct

A. M. K. P. Taylor, J. H. Whitelaw,
and M. Yianneskis

CONTRACT NASW-3435
MAY 1982

NASA

NASA Contractor Report 3550

Developing Flow in S-Shaped Ducts

I - Square Cross-Section Duct

A. M. K. P. Taylor, J. H. Whitelaw,
and M. Yianneskis
Imperial College of Science and Technology
London, England

Prepared for
NASA Headquarters
under Contract NASW-3435

National Aeronautics
and Space Administration

**Scientific and Technical
Information Office**

1982

TABLE OF CONTENTS

SUMMARY

The secondary flows in a square-section S-duct have been measured at five stations within the duct for Reynolds numbers of 790 and 40 000 in a water tunnel. The S-duct was formed from two 22.5° bends with 40 mm hydraulic diameter and 280 mm mean radius of curvature. The boundary layers at the inlet to the duct were approximately 25% and 15% of the hydraulic diameter for the laminar and turbulent results respectively. Laser-Doppler velocimetry was used to measure velocities in the plane of curvature and, in turbulent flow, to measure the associated fluctuations and cross-correlations. For turbulent flow, wall pressure distributions are also reported.

In the first bend, pressure driven secondary flows are formed and are larger in the laminar flow case. This difference between the two flow regimes is due partly to the difference in the boundary layer thickness at the inlet. On passing into the second bend, the imposed radial pressure gradients give rise to forces which oppose the original streamwise vorticity except for one region near the outer wall where the existing streamwise vorticity is sustained, according to the Squire-Winter result, because of the local sign of the radial vorticity. On exit from the duct, the secondary flow over most of the section is in the opposite direction to that in the first half although the net redistribution of the streamwise isotachs is comparable to that in unidirectional bends of stronger curvature.

An important objective of this work is to provide observations in sufficient detail and accuracy for the evaluation of numerical calculation methods. Accordingly, the measurements are presented in tabular form and are also available on magnetic tape for ease of reference.

1. INTRODUCTION

S-shaped ducts and passages occur in a multitude of practical applications, where a combination of bends is employed to re-direct the flow. Typical applications are found in aircraft with dorsal or wing-root intakes, such as those used in the Lockheed L-1011, the Boeing 727 and in V/STOL aircraft which employ considerable re-direction of the engine thrust. Other applications include internal combustion engine passages. The generation of cross-stream secondary flows due to the curvature of the duct can influence significantly the flow at its exit. The performance of the engines is very sensitive to intake losses, and knowledge of how to minimise pressure losses, reduce flow distortion and maximise the flow rate is essential in order to improve the engine's efficiency. In environmental flows, such as that in river bends, the generation of secondary flow enhances the meandering of river beds because of the deposition of silt on the inside and the erosion of the outside of the bend.

Measurements and calculations of total pressure and yaw angle in a $45^{o}/45^{o}$ and a $30^{o}/30^{o}$ S-shaped pipe of mild curvature have been reported in reference 1 for fully developed inlet flow. It was observed that the flow in an S-bend is characterised by total pressure gradients (in the direction normal to the plane of the bend) which sustain the motion generated in the first bend. The low-pressure region, generated in the first half of the S-duct, was observed to spread over the centre of the pipe in the second half. The measurements of reference 2 in strongly-curved S-shaped pipes with thin inlet boundary layers indicated the existence of a pair of contra-rotating vortices within this low-pressure region on exit from the pipes. These were attributed to the production of streamwise vorticity in the first bend and vortex stretching towards the end of the second bend. Two-dimensional flow measurements in rectangular $30^{o}/45^{o}$ and $45^{o}/45^{o}$ S-ducts were reported in reference 3, and the results show a potential-type flow in the duct's symmetry plane.

A square duct was used in this investigation, to provide a fully three-dimensional flow, with thin inlet boundary layers, relatively mild curvature and small centre-line displacement. The last two conditions reduce the likelihood of flow separation at the walls of the duct and thus there exists a primary flow direction which makes its numerical calculation amenable to marching techniques. Measurements of the velocity characteristics of both laminar and turbulent flow regimes are reported. The laminar and turbulent flow results can be used to assess the numerical accuracy of calculation techniques and the suitability of turbulence models respectively. In order to provide accurate, non-intrusive flow measurements, laser-Doppler velocimetry was used. These measurements are the extension of an earlier investigation into the secondary flows in 90^{o} bends (reference 4) and the interest in the observations reported here lies principally in examining the behaviour of the flow in the second bend which forms the S-duct.

A description of the flow configuration with a brief account of the experimental procedure is given in the following section. Laminar and turbulent

results are presented successively in section 3 and discussed in section 4. The report closes with a list of conclusions.

2. FLOW CONFIGURATION AND INSTRUMENTATION

2.1 Flow Configuration

The duct, shown in figure 1, was constructed from two square cross-sectioned 22.5° bends cut from a single 90° bend with ratio of the mean radius of curvature to the hydraulic diameter of 7. The two bends were clamped tightly together to form the inflexion plane of the S-duct across which there was no gap or discontinuity in the duct walls. The ratio of the overall duct length to the centre-line displacement was 5.2. The mean radius of the bends was 280 mm, and the dimensions of the cross-section ($40 \pm 0.1 \times 40 \pm 0.1$ mm) were identical to those used in reference 5.

The coordinate system is also shown in figure 1. Streamwise distance is measured along the centre-line in hydraulic diameters (D_H = 0.04 m) from the inlet plane of the first bend. The duct was located downstream of a 12:1 contraction with honeycomb flow straighteners and a boundary layer trip of 0.5 mm. An upstream entry length of 0.3 m (7.5 D_H) and a downstream tangent of 2.0 m (50 D_H) were used.

The water tunnel was identical, apart from the test section, to that used in reference 4. The flow rate was measured by precision bore flowmeters. Experiments were made at two Reynolds numbers, 790 and 40 000 for the laminar and turbulent flows, corresponding to Dean numbers, $De = Re\ (\frac{1}{2}\ D_H/R_C)^{\frac{1}{2}}$, of 212 and 10690 respectively. Water was employed as the working fluid so that the same Reynolds numbers could be obtained at a smaller scale than that achieved in air, and to allow a high measurement accuracy. The occurrence of natural contaminants in the water provided seeding for the velocimeter. However, minute quantities of milk were added to the water to increase the scattering particle concentration. In order to ensure that there was no appreciable change in the viscosity, and therefore in the flow rate, the water temperature was maintained at $20° \pm 2°C$ throughout the experiments.

2.2 Laser Doppler Velocimeter, Experimental Procedure and Accuracy

The optical and signal processing arrangements of the velocimeter were practically identical to those used in reference 4 and are not described in

this report. Measurements were made in three directions, ($0^o \pm 45^o$) in the X-r* plane at each measurement point with the beams entering through the side-wall and the Doppler frequencies were resolved to provide the local streamwise (U, $\bar{U}$ and $\tilde{u}$) and radial (V, $\bar{V}$ and $\tilde{v}$) components and the $\overline{uv}$ cross-correlations in the manner described in reference 5. The spanwise component was measured with the beams entering through the wall at r*=1 in the r*-z* plane. The curvature of the wall prohibited measurements at $\pm 45^o$ in the X-z* plane, as the beams will only cross if they lie in the r*-z* or the X-z* (0^o) planes. The alignment of the beams perpendicular to the curved wall at the cross-sections of interest was achieved by mounting the optics on a rotating lathe table in addition to the three-dimensional translating table. The thickness of the duct side walls restricted optical access and thus the extent of the measurement grid in the r*-z* plane.

The small magnitude of the spanwise component necessitated the use of frequency shifting. The radial diffraction grating, used solely as a beam splitter for the U and V component measurements, could be rotated with a variable speed motor to provide light frequency shifts between the first-order diffracted beams in the range 0.25 - 1.50 MHz. As the minimum shift obtainable was 0.25 MHz spanwise measurements could be made only for the turbulent case. Owing to the difficulties of obtaining rotational stability at the low speeds, a fly-wheel was added to the motor shaft to increase the inertia of the grating. A frequency shift of 0.285 MHz was applied for all the spanwise component measurements.

The principal characteristics of the optical system are given in the table below:

Characteristics of the optical arrangement

Focal length of imaging lens (mm)	200
Half-angle of intersection	9.3^o
Fringe separation (line-pair spacing)	2 μm
Number of fringes in measuring volume	86
Intersection volume diameter calculated at $1/e^2$ intensity (mm)	0.167
Intersection volume length calculated at $1/e^2$ intensity (mm)	1.357
Photomultiplier pinhole diameter (mm)	0.50
Transfer constant (MHz/ms^{-1})	0.510

Detailed estimates of accuracy (systematic error) and precision (random error) for the velocity measurements are given in reference 4. Systematic errors are generally of the order of 1% rising to 2-3% in the regions of

steep velocity gradients near the walls. The random error associated with the instability of the rotating grating speed is of the order of 0.005 of the bulk velocity.

Measurements were made at five streamwise stations in the duct, as shown in Figure 1, namely at 0.0 (inlet plane), 1.65, 2.50, 3.85 and 5.50 (exit plane) hydraulic diameters from the entry plane of the S-duct. These correspond to 0^o, 13.5^o and 20.5^o from the duct entrance in the first bend, and to 13.5^o and 0^o from the duct exit in the second bend.

Wall pressure measurements were obtained through pressure tappings let into the duct walls. A conventional water micro-manometer was used for the turbulent flow measurements. A second manometer, accurate to 10 μm of water column, was used for the laminar flow measurements; the pressure differences were of this order and thus only an indication of their magnitude could be obtained. Pressure measurements were made at six streamwise stations, located 1.1, 2.2, 3.3 and 4.4 hydraulic diameters from the duct entrance within the duct, at 1.0 D_H upstream of the entry and 1.0 D_H downstream of the exit.

A qualitative description of the flow was obtained with visualization using hydrogen bubbles produced on 0.375 mm Nichrome and 0.08 mm Platinum wires inserted through the pressure tappings. Observation of the flow visualization for the lower of the two Reynolds numbers confirmed the laminar and steady nature of the flow.

3. RESULTS

3.1 Laminar Flow Results

The flow features are qualitatively indicated in the photographs of figure 2, which were taken at a Reynolds number of 1275. Figure 2(i) shows the hydrogen bubbles, produced by a wire inserted at 1 D_H upstream of the entry, following the high velocity "core" flow which moves in a S-shaped path, migrating somewhat towards the outer wall of the first bend. The secondary flow pattern along the side walls is shown in figure 2(ii) by the bubbles which have accumulated on the top side wall; the flow is directed towards the inner wall of the first bend and after the plane of inflection is re-directed towards the opposite wall due to the change in the direction of the pressure gradient in the second bend. The core flow is again observed to follow an S-shaped path with a small displacement away from the duct's centre-line to the inner wall of the second bend (from $r^* = 0.5$ at $X_H = 1.1$, where the bubbles are produced, to $r^* = 0.3$ at $X_H = 4.4$).

Measurements on both sides of the symmetry plane showed that the flow in both regimes was symmetrical to within the precision of the measurements.

The streamwise and gapwise velocities normalised by V_b are shown in contour and profile form in figures 3-6. The flow entering the duct is nearly symmetric, with boundary layer thickness, defined at 0.95 of the maximum velocity, of 25% of the hydraulic diameter. All contours presented in the report have been drawn using linear interpolation between the measurement grid (5 x 12) which is defined by the profiles shown and the inner and outer walls of each bend are marked on each contour plot.

The streamwise isotachs show the high velocity core flow being displaced, on entry to the first bend, towards the outer wall (figure 3(ii) and (iii)). By the exit of the first bend (figure 3(iii)) the accumulation of low speed fluid near the inner wall, a characteristic of secondary motion, is evident. The radial component of velocity at the entrance to the first bend, shown in figure 5(i), is directed towards the inner wall as expected (see reference 4) but develops into a vortex within the bend (figures 5(ii) and (iii)). The maximum measured component was 0.22 of the bulk velocity. On passing into the second bend (figures 3(iv) and (v)),the movement of core flow towards the wall at r*=0 (now the inner wall) is retarded and eventually reversed, while the side-wall boundary layers (the source of vorticity for the generation of streamwise vorticity) become substantially thinner. By the exit of the S-duct there is a large region of low streamwise velocity fluid near the outer (r*=1.0) wall of the bend which is comparable to that existing in a unidirectional bend after 60^{o} of turning with a smaller radius ratio (2.3) (see reference 4). This is notable because intuitively one might expect that a smaller total angle of turning (in this case 22.5^{o} and 22.5^{o}) with a larger radius ratio (in this case 7.0) would result in a substantially smaller region of low speed fluid being created. This point is addressed further in the discussion. In the second bend, the radial component of velocity is initially (figure 5(iv)) reduced in magnitude, compared to the previous measurement station particularly near the side-walls, and has reversed its direction only in the region adjacent to the inner wall of the bend. This reversal extends over a greater area of the cross-section in the final station (figure 5(v)) but is not complete near the inner wall (i.e. at r*=0.9 and 0.7, z*<0.4). The maximum measured radial component is only 0.10 of the bulk velocity in the second bend.

The measured values are provided in Appendix I as Table 1.

3.2 Turbulent Flow Results

Measurements of the mean velocity streamwise, radial and spanwise components are shown in Figures 7-12. Wall pressure measurements are shown in Figure 13; the cross-correlations and turbulence quantities are presented in figures 11 and 14-16.

The streamwise isotachs present a flow development markedly different from that of the laminar case. The flow at the inlet (figure 7(i)) shows the "core" flow located nearer the inner wall of the first bend. This is associated with the thinner boundary layers at entry (0.15 D_H at 0.95 of maximum velocity), and the resulting smaller secondary flows, with development reminiscent of a potential (i.e. irrotational) flow near the symmetry plane. This is particularly evident at the 2nd station, where the velocity maximum is located at $r^* = 0.7$ (figure 7(ii)) (see references 4 and 6 for a discussion). Subsequently the high velocity "core" moves towards the outer wall under the influence of the steadily strengthening secondary flow. This displacement persists in the second bend (figure 7(iv)) and the first evidence of the effects of streamwise vorticity (indicated by the migration of the core towards the inner wall) can be observed in figure 7(iv). As for the laminar flow, the sidewall boundary layers become much thinner by this station as compared to the value at the inlet to the S-duct. By the exit of the duct, figure 7(v), the core has moved towards the centre of the duct and the distortion of the isotachs is more pronounced near the outer wall. The region of low velocity fluid which has accumulated at the exit of the S-duct (near the outer wall of the second bend) is much smaller than for the laminar flow counterpart. The distortion is comparable, however, to that existing in turbulent flow in a unidirectional bend of stronger curvature, after larger angles of turning (reference 4).

The radial velocity component measurements shown as profiles in figure 9 and contours in figure 10 are entirely consistent with the observations of the streamwise component results. The flow development in the cross-stream plane is found to be similar to that of the laminar case, but with smaller velocity magnitudes. The radial components, initially directed towards the inner wall with magnitudes less than 0.04 V_b, figure 9(i) , become near-zero in the "core" flow region at the 2nd station, rising near the side-wall to about 0.10 V_b. The onset, and effect, of the secondary flow is thus delayed in the turbulent flow case; maximum velocities of 0.15 V_b are reached in the 3rd station, being approximately two-thirds of those in the laminar case. These magnitudes are, however, smaller than those in the 90° bend of similar curvature of reference 7, which were 0.20 V_b at 45° around the bend.

The reversal of the direction of the secondary flow in the second bend, mentioned in the previous subsection, is also observed at station 5 although, as for the laminar flow, the direction of the radial velocity at this station (figure 5(v)) at $r^* = 0.9$, $z^* \simeq 0$ remains unchanged from that in the first bend. The change in direction is also not complete even at $r^* = 0.5$, $z^* < 0.4$ and these observations form an important point of the discussion below.

The spanwise mean velocity components are shown in figures 11 and 12(i), (iii) and (v) as contours and profiles respectively. Measurements of this component were only made up to $z^* \simeq 0.5$ because of restricted optical access near the side-walls. The contour and profile plots extend up to $z^* = 0.5$

for uniformity. The components shown as positive indicate a direction of motion away from the side-wall and towards the symmetry plane. Spanwise measurements in the inlet and exit planes were not possible as locating screws prohibited optical access. The measurements show that the flow has a counter-clockwise rotation, as viewed in the plane of figure 12, which is consistent with the direction deduced from the radial components up to the location $X_H = 3.85$. The maximum magnitude of the spanwise component ($\simeq 0.06$ of the bulk velocity) is smaller than that of the radial component.

The wall pressure measurements are presented as functions of the streamwise and radial directions in figures 13(i) and (ii) respectively. The radial pressure gradient extends up to about one hydraulic diameter upstream and downstream of the duct. The pressure gradients set up by each bend can be distinguished and are separated very near the inflexion plane. The pressure loss across the duct is approximately one tenth of the velocity head, nearly half of that measured in the 90^0 bend of reference 4. The favourable gradient on the inner wall at the duct entrance is significantly stronger than the adverse one on the outer wall. Upon entry to the second bend the favourable gradient is again more significant than the adverse one on the opposite wall. The diagrams for both bends are very similar, being almost anti-symmetric about the plane of inflexion.

The $\overline{uv}$ cross-correlations are presented in figure 14. The measured values have maxima approaching $0.003\ V_b^2$ in the outer wall ($r^* = 0$) region of the first bend, and near the side-walls. In the core flow region values are near-zero and within experimental scatter. The changes in the gradient $\partial U/\partial r$ conform closely with the changes in the sign of $\overline{uv}$, as for example on either side of the duct in station 4.

The turbulence levels for the streamwise, radial and spanwise components are shown, as contours, in figures 15, 16 and 11 respectively. The streamwise levels rise to about $0.13\ V_b$ near the side-walls and the radial levels to about $0.08\ V_b$; spanwise levels of up to $0.06\ V_b$ were measured in the central part. In the core region very weak levels exist, in general below $0.02\ V_b$. The contours of the levels in all three directions show similarities, with larger values occurring near the inner wall ($r^* = 1.0$) where significant streamwise velocity gradients are present.

The velocity and turbulence results are tabulated in the Appendix as Table 2 and the wall pressure measurements as Table 3.

4. DISCUSSION

The generation of streamwise vorticity is an inviscid process, given an initial boundary layer (see, for example, reference 2). The laminar or turbulent nature of the flow influences the rate at which new cross-stream vorticity is generated at the side-walls, to replace that which is removed by the secondary flow, and also directly affects the streamwise vorticity through the induced (laminar or turbulent) shear stresses, particularly near the side-walls. The first consideration leads to the conclusion that the differences between the two flow regimes is strongly influenced by the initial difference in the boundary layer thickness (that is, the initial cross-stream vorticity) at the entrance to the duct.

The laminar flow, with the thicker boundary layer at the inlet to the S-duct, thus gives rise to stronger cross-stream flows than does the turbulent flow. The qualitative development within the first bend is very similar to that in the same region of a square cross-section, 90^{o} bend of 2.3 radius ratio, which has been discussed extensively in previous publications (references 4 and 6). It is noted that the turbulent flow development in the first bend of the S-duct is not the same as that mentioned in reference 6 for a 90^{o} bend of radius ratio 7.0 because the pressure gradient which exists in the first bend of the S-duct is quite different to that in the first twenty or so degrees of the 90^{o} bend.

The passage of the flow into the second bend brings it under the influence of a radial pressure gradient which is opposite in direction to that of the first bend, due to the change in the radius of curvature. The reversal in the sign of the pressure gradient gives rise to forces which oppose the cross-stream motion present at the end of the first bend and thus begins to attenuate this motion. These forces eventually not only eradicate the original vorticity but, by the end of the second bend, have established a vortex rotating in the opposite sense.

Towards the outer wall of the second bend, however, this description does not apply because of the redistribution of the streamwise isotachs, caused by the secondary flow established in the first bend. The reason for this can be shown by considering the Squire & Winter formula (reference 7) for the production of streamwise vorticity from cross-stream vorticity:

$$\delta \left(\frac{\partial W}{\partial r'} - \frac{\partial V}{\partial z}\right) = -2 \left(\frac{\partial U}{\partial z} - \frac{\partial W}{\partial \theta}\right) \delta\theta \qquad (1)$$

{note: r' is the radial co-ordinate directed towards the centre of curvature in each bend}.

The equation relates the magnitude and direction of the streamwise vorticity to that existing in the radial direction. Since $\partial W/\partial\theta << \partial U/\partial z$, the direction of the streamwise vorticity vector which is generated depends on the sign of $\partial U/\partial z$.

Examination of figures 3(iv) and 7(iv) and particularly 3(v) and 7(v) shows that $\partial U/\partial z$ changes sign at $z^* \simeq 0.5$, $0.7 \lesssim r^* \lesssim 0.9$ and equation (1) shows that the streamwise vorticity generated by the first bend in this region will be reinforced, not attenuated, by passage through the second bend. This explains the persistence of the original radial velocity direction near the inner wall, noted in the presentation of the results in sub-sections 3.1 and 3.2. Reference 1 drew attention to this process in S-duct flows and the measurements of the radial components, presented in section 3, provide confirmation. As noted in reference 1, and sub-section 3.1, this local reinforcement of the initial vorticity in the second half of an S-duct gives rise to similar, or even greater, redistribution of the streamwise isotachs at the end of the S-duct as compared with unidirectional bends of the same total turning angle.

The effects of cross-sectional shape on the secondary flows is discussed in the companion report (part II) which presents measurements in a similar S-duct but of circular section.

The turbulence levels, $\tilde{u}$ and $\tilde{v}$ are similar to those which have been measured (reference 6) in the 90^o bends of 2.3 and 7.0 radius ratio and so are the $\overline{uv}$ cross-correlations. The values are those expected to exist in a relatively unstrained core interacting with the wall boundary layers and are only of importance to the flow development in regions very close to the side-walls.

5. CONCLUDING REMARKS

1. This report presents, in detail, the velocity characteristics of laminar and turbulent developing flow in a S-duct formed from two 22.5^o sectors of a bend of rectangular cross-section.

2. Pressure-driven secondary flows arise in the first bend of the duct and reach measured maxima of 0.22 and 0.15 of the bulk velocity in the laminar and turbulent flows respectively. The velocities are greater in the laminar flow mainly because of the thicker inlet boundary layers. On passing through the second half of the S-duct, a secondary flow is established over most of the section in the opposite direction to that in the first half.

3. Near the outer wall of the second bend, however, the secondary flow which was generated in the first bend is sustained because of the local sign of the radial vorticity. This effect contributes to a redistribution of the streamwise isotachs, by the end of the duct, comparable to that in unidirectional bends.

4. This report presents benchmark measurements against which the results of numerical calculation methods can be compared.

APPENDIX 1

TABULATED DATA

T A B L E 1

LAMINAR FLOW VELOCITIES; RE=790

ALL QUANTITIES NORMALISED WITH THE BULK VELOCITY, 0.0198 M/S

NOTE: gapwise direction is radial direction.

LAMINAR FLOW STREAMWISE VELOCITIES; STATION 1

R*=	0.1	0.3	0.5	0.7	0.9
Z*=					
0	.817	1.500	1.605	1.565	.938
.100	.813	1.500	1.605	1.565	.917
.200	.798	1.500	1.605	1.565	.907
.300	.770	1.500	1.601	1.561	.891
.400	.736	1.480	1.593	1.544	.867
.500	.698	1.440	1.561	1.508	.835
.600	.663	1.375	1.492	1.427	.790
.700	.605	1.194	1.343	1.290	.708
.800	.516	.895	.988	.984	.518
.900	.333	.548	.619	.597	.341
.925	.298	.448	.440	.524	.276
.950	.228	.302	.323	.383	.214

LAMINAR FLOW STREAMWISE VELOCITIES; STATION 2

R*=	0.1	0.3	0.5	0.7	0.9
Z*=					
0	1.014	1.573	1.573	1.472	.674
.100	1.012	1.573	1.573	1.457	.668
.200	1.008	1.573	1.573	1.431	.655
.300	.998	1.573	1.573	1.411	.629
.400	.988	1.552	1.532	1.391	.601
.500	.970	1.452	1.452	1.331	.595
.600	.885	1.371	1.331	1.230	.611
.700	.740	1.210	1.149	1.089	.573
.800	.585	.927	.897	.786	.492
.900	.335	.556	.538	.516	.315
.925	.292	.446	.444	.433	.262
.950	.218	.337	.333	.300	.181

LAMINAR FLOW STREAMWISE VELOCITIES; STATION 3

R*=	0.1	0.3	0.5	0.7	0.9
Z*=					
0	1.311	1.653	1.613	1.210	.524
.100	1.311	1.653	1.613	1.210	.524
.200	1.311	1.633	1.603	1.210	.482
.300	1.311	1.633	1.583	1.169	.442
.400	1.311	1.613	1.542	1.149	.454
.500	1.280	1.552	1.492	1.129	.514
.600	1.210	1.492	1.411	1.089	.585
.700	1.131	1.391	1.270	1.058	.540
.800	.944	1.230	1.125	.897	.435
.900	.696	.950	.746	.579	.274
.925	.577	.754	.681	.524	.228
.950	.520	.639	.514	.387	.177

LAMINAR FLOW STREAMWISE VELOCITIES; STATION 4

R*=	0.1	0.3	0.5	0.7	0.9
Z*=					
0	1.593	1.744	1.280	.825	.357
.100	1.593	1.744	1.331	.837	.359
.200	1.573	1.744	1.361	.786	.355
.300	1.552	1.724	1.391	.745	.349
.400	1.512	1.714	1.421	.799	.373
.500	1.472	1.673	1.442	.911	.442
.600	1.391	1.633	1.442	.984	.496
.700	1.270	1.573	1.401	.933	.472
.800	1.069	1.472	1.280	.752	.373
.900	.857	1.125	.867	.472	.250
.925	.766	1.008	.714	.377	.232
.950	.613	.766	.552	.327	.163

LAMINAR FLOW STREAMWISE VELOCITIES; STATION 5

R*=	0.1	0.3	0.5	0.7	0.9
Z*=					
0	.756	1.794	1.431	.742	.671
.100	.756	1.774	1.421	.728	.488
.200	.750	1.774	1.401	.718	.389
.300	.718	1.792	1.361	.750	.425
.400	.702	1.784	1.311	.831	.532
.500	.669	1.784	1.331	1.000	.675
.600	.712	1.734	1.452	1.165	.823
.700	.810	1.683	1.482	1.173	.778
.800	.770	1.583	1.311	.938	.617
.900	.542	1.026	.865	.526	.429
.925	.429	.851	.730	.438	.313
.950	.399	.643	.591	.345	.202

LAMINAR FLOW GAPWISE VELOCITIES; STATION 1

R*=	0.1	0.3	0.5	0.7	0.9
Z*=					
0	.013	.040	.037	.017	0
.100	.010	.040	.037	.017	.001
.200	.020	.040	.037	.017	.001
.300	.017	.040	.037	.021	.001
.400	.014	.029	.031	.029	0
.500	.017	.034	.029	.029	.001
.600	.014	.023	.026	.031	.007
.700	.013	.009	.026	.031	.014
.800	.014	.006	.026	.026	.021
.900	.016	0	.023	.023	.031
.925	.013	0	.009	.020	.029
.950	.013	0	.009	.003	.019

LAMINAR FLOW GAPWISE VELOCITIES; STATION 2

R*=	0.1	0.3	0.5	0.7	0.9
Z*=					
0	-.021	-.114	-.128	-.143	-.038
.100	-.021	-.128	-.128	-.143	-.033
.200	-.021	-.128	-.128	-.143	-.038
.300	-.014	-.128	-.128	-.128	-.038
.400	-.013	-.114	-.128	-.128	-.041
.500	-.009	-.091	-.114	-.100	-.034
.600	.013	-.057	-.086	-.071	-.026
.700	.026	0	-.014	-.014	.013
.800	.047	.114	.143	.114	.050
.900	.061	.172	.187	.163	.071
.925	.060	.171	.181	.157	.057
.950	.053	.133	.153	.120	.043

LAMINAR FLOW GAPWISE VELOCITIES; STATION 3

R*=	0.1	0.3	0.5	0.7	0.9
Z*=					
0	-.043	-.171	-.214	-.185	-.033
.100	-.043	-.171	-.214	-.185	-.033
.200	-.043	-.171	-.207	-.185	-.031
.300	-.043	-.171	-.200	-.171	-.037
.400	-.043	-.171	-.185	-.171	-.051
.500	-.043	-.128	-.157	-.157	-.038
.600	0	-.071	-.100	-.086	-.007
.700	.023	-.043	-.014	.031	.029
.800	.051	.061	.131	.138	.054
.900	.083	.165	.202	.170	.046
.925	.087	.200	.195	.150	.047
.950	.086	.218	.180	.111	.033

LAMINARFLOW GAPWISE VELOCITIES; STATION 4

R*=	0.1	0.3	0.5	0.7	0.9
Z*=					
0	.057	-.014	-.064	-.029	-.003
.100	.057	-.014	-.043	-.013	-.001
.200	.057	-.014	-.021	-.031	-.003
.300	.057	-.014	-.029	-.047	.006
.400	.057	-.014	-.014	-.033	.011
.500	.071	0	.007	.003	.024
.600	.086	.043	.036	.064	.031
.700	.086	.086	.110	.120	.037
.800	.086	.157	.200	.102	.010
.900	.014	.138	.127	.024	-.013
.925	.011	.133	.102	.001	-.009
.950	.007	.093	.061	.001	-.003

LAMINAR FLOW GAPWISE VELOCITIES; STATION 5

R*=	0.1	0.3	0.5	0.7	0.9
Z*=					
0	.073	.114	.086	0	-.026
.100	.073	.100	.086	-.006	-.037
.200	.071	.107	.071	-.010	-.036
.300	.068	.114	.057	-.006	-.007
.400	.061	.114	.057	.004	.014
.500	.066	.121	.057	.074	.021
.600	.064	.153	.100	.145	.090
.700	.038	.150	.150	,170	.061
.800	-.026	.128	.128	.090	.006
.900	-.076	-.031	-.014	-.031	-.023
.925	-.078	-.100	-.038	-.040	-.047
.950	-.060	-.086	-.064	-.050	-.037

TABLE 2

TURBULENT FLOW VELOCITIES, TURBULENCE LEVELS AND CROSS CORRELATIONS; RE=40,000

MEAN VELOCITIES AND TURBULENCE LEVELS NORMALISED WITH THE BULK VELOCITY, 1 M/S;
CROSS CORRELATIONS NORMALISED WITH THE SQUARE OF THE BULK VELOCITY

TURBULENT FLOW STREAMWISE MEAN VELOCITIES; STATION 1

R*=	0.1	0.3	0.5	0.7	0.9
Z*=					
0	.982	1.130	1.142	1.148	1.010
.100	.986	1.130	1.142	1.148	1.014
.200	.982	1.130	1.142	1.148	1.014
.300	.980	1.130	1.142	1.148	1.014
.400	.984	1.130	1.142	1.148	1.014
.500	.982	1.126	1.134	1.148	1.010
.600	.985	1.110	1.120	1.138	1.006
.700	.970	1.038	1.058	1.110	1.002
.800	.905	.962	.966	1.006	.890
.900	.856	.846	.814	.846	.756
.925	.812	.758	.715	.778	.647
.950	.693	.647	.659	.754	.517

TURBULENT FLOW STREAMWISE MEAN VELOCITIES; STATION 2

R*=	0.1	0.3	0.5	0.7	0.9
Z*=					
0	.934	1.078	1.134	1.162	1.022
.100	.934	1.078	1.134	1.162	1.010
.200	.934	1.082	1.134	1.162	1.006
.300	.934	1.074	1.134	1.158	1.006
.400	.934	1.074	1.134	1.158	1.014
.500	.934	1.074	1.130	1.154	1.014
.600	.934	1.062	1.082	1.126	1.018
.700	.922	1.018	1.030	1.074	1.010
.800	.906	.918	.958	.978	.946
.900	.826	.790	.822	.862	.830
.925	.794	.790	.790	.826	.758
.950	.719	.707	.750	.766	.731

TURBULENT FLOW STREAMWISE MEAN VELOCITIES; STATION 3

R*=	0.1	0.3	0.5	0.7	0.9
Z*=					
0	.998	1.142	1.158	1.154	.930
.100	.998	1.142	1.158	1.154	.926
.200	.998	1.146	1.158	1.158	.926
.300	.998	1.142	1.158	1.150	.922
.400	.998	1.144	1.156	1.152	.922
.500	.996	1.132	1.136	1.146	.932
.600	.990	1.074	1.090	1.110	.934
.700	.973	1.008	.998	1.058	.892
.800	.918	.970	.970	.974	.834
.900	.826	.882	.856	.862	.651
.925	.758	.818	.798	.750	.519
.950	.611	.623	.647	.703	.423

TURBULENT FLOW STREAMWISE MEAN VELOCITIES; STATION 4

R*=	0.1	0.3	0.5	0.7	0.9
Z*=					
0	1.118	1.198	1.178	1.042	.699
.100	1.118	1.198	1.178	1.042	.679
.200	1.118	1.206	1.174	1.038	.651
.300	1.118	1.198	1.174	1.038	.627
.400	1.118	1.198	1.174	1.034	.655
.500	1.118	1.194	1.170	1.026	.727
.600	1.118	1.182	1.134	1.014	.792
.700	1.098	1.150	1.078	.978	.802
.800	1.071	1.102	1.002	.930	.778
.900	1.034	1.048	.914	.830	.695
.925	1.014	1.014	.880	.802	.655
.950	.978	.970	.842	.754	.583

TURBULENT FLOW STREAMWISE MEAN VELOCITIES; STATION 5

R*=	0.1	0.3	0.5	0.7	0.9
Z*=					
0	1.054	1.170	1.218	1.062	.719
.100	1.056	1.178	1.210	1.056	.689
.200	1.056	1.174	1.214	1.052	.695
.300	1.058	1.190	1.208	1.044	.745
.400	1.054	1.190	1.198	1.058	.818
.500	1.054	1.194	1.194	1.070	.868
.600	1.026	1.180	1.176	1.058	.906
.700	1.022	1.162	1.112	1.030	.902
.800	.976	1.116	.994	.958	.830
.900	.922	.948	.858	.792	.699
.925	.834	.878	.756	.739	.619
.950	.677	.681	.601	.571	.495

TURBULENT FLOW GAPWISE MEAN VELOCITIES; STATION 1

R*=	0.1	0.3	0.5	0.7	0.9
Z*=					
0	.020	.034	.040	.017	.008
.100	.020	.034	.040	.017	.008
.200	.025	.034	.040	.017	.008
.300	.025	.034	.038	.017	.006
.400	.024	.034	.034	.017	.020
.500	.020	.031	.034	.023	.014
.600	.017	.023	.031	.025	.017
.700	.011	.017	.028	.028	.014
.800	.008	.020	.025	.045	.025
.900	.008	.020	.025	.042	.023
.925	.006	.023	.020	.051	.034
.950	0	.014	.011	.065	-.006

TURBULENT FLOW GAPWISE MEAN VELOCITIES; STATION 2

R*=	0.1	0.3	0.5	0.7	0.9
Z*=					
0	0	.006	-.008	-.003	.011
.100	.006	.006	-.003	-.006	.011
.200	.010	.003	-.008	-.008	.006
.300	.008	.003	-.008	-.006	.003
.400	.006	.003	-.011	-.011	0
.500	.003	-.008	-.011	-.011	.011
.600	.006	-.011	-.003	-.003	.011
.700	.008	.006	.025	.011	.020
.800	.023	.034	.051	.056	.031
.900	.037	.085	.110	.102	.061
.925	.042	.110	.121	.110	.078
.950	.049	.133	.133	.109	.073

TURBULENT FLOW GAPWISE MEAN VELOCITIES; STATION 3

R*=	0.1	0.3	0.5	0.7	0.9
Z*=					
0	-.011	-.068	-.079	-.082	-.037
.100	-.014	-.062	-.079	-.083	-.034
.200	-.017	-.065	-.085	-.085	-.037
.300	-.028	-.066	-.085	-.082	-.040
.400	-.030	-.069	-.087	-.079	-.040
.500	-.025	-.072	-.085	-.079	-.037
.600	-.027	-.048	-.045	-.062	-.025
.700	-.011	0	.014	-.030	-.009
.800	.017	.044	.086	.021	.033
.900	.034	.121	.118	.087	.073
.925	.062	.152	.134	.095	.035
.950	.071	.140	.083	.102	.042

TURBULENT FLOW GAPWISE MEAN VELOCITIES; STATION 4

R*=	0.1	0.3	0.5	0.7	0.9
Z*=					
0	.045	.023	.011	-.004	.006
.100	.040	.023	.008	0	.009
.200	.034	.023	.008	-.003	.006
.300	.031	.023	.008	0	-.008
.400	.028	.023	.007	.006	-.001
.500	.028	.023	.008	.011	.025
.600	.025	.025	.018	.017	.037
.700	.025	.035	.040	.037	.068
.800	.045	.062	.082	.079	.079
.900	.042	.087	.110	.099	.073
.925	.038	.102	.110	.099	.061
.950	.040	.100	.096	.087	.032

TURBULENT FLOW GAPWISE MEAN VELOCITIES; STATION 5

R*=	0.1	0.3	0.5	0.7	0.9
Z*=					
0	.030	.040	.008	-.003	-.011
.100	.020	.044	.007	-.003	-.037
.200	.028	.054	.010	-.007	-.045
.300	.032	.037	.004	-.004	-.023
.400	.025	.040	.002	.006	.008
.500	.030	.031	.011	.017	.030
.600	.025	.037	.014	.028	.045
.700	.025	.038	.028	.037	.049
.800	-.021	.037	.011	.025	.021
.900	-.051	-.031	-.025	-.042	-.042
.925	-.092	-.071	-.068	-.062	-.102
.950	-.123	-.134	-.111	-.096	-.122

SPANWISE VELOCITIES; STATION 2

R*=	0..	0.3	0.5	0.7	0.8
Z*=					
0	0	0	0	.002	0
.100	-.008	-.004	0	.004	.004
.200	-.010	-.004	0	.007	.012
.300	-.012	-.008	0	.008	.023
.400	-.012	-.008	0	.008	.028
.500	-.020	-.012	.004	.011	.038
.600	-.028	-.018	.004	.012	
.700	-.032				

SPANWISE TURBULENCE LEVELS; STATION 2

R*=	0.1	0.3	0.5	0.7	0.8
Z*=					
0	.033	.011	.010	.010	.038
.100	.031	.011	.008	.008	.040
.200	.048	.012	.008	.010	.041
.300	.047	.012	.010	.011	.038
.400	.031	.013	.013	.014	.038
.500	.052	.018	.018	.018	.041
.300	.054	.023	.027	.018	
.700	.054				

SPANWISE VELOCITIES; STATION 3

R*=	0.1	0.3	0.5	0.7	0.8
Z*=					
0	0	.002	0	0	0
.100	-.004	-.008	0	0	.008
.200	-.010	-.008	-.004	0	.020
.300	-.013	-.018	-.008	0	.032
.400	-.017	-.013	-.008	.004	.044
.500	-.020	-.025	-.004	.008	.048
.600	-.030	-.028	-.004	.008	
.700	-.034	-.044			

SPANWISE TURBULENCE LEVELS; STATION 3

R*=	0.1	0.3	0.5	0.7	0.8
Z*=					
0	.032	.008	.011	.011	.042
.100	.048	.008	.008	.011	.044
.200	.047	.011	.008	.012	.045
.300	.042	.010	.011	.014	.043
.400	.047	.013	.011	.015	.048
.500	.048	.013	.020	.025	.045
.600	.033	.020	.027	.030	
.700	.058	.021			

SPANWISE VELOCITIES; STATION 4

R*=	0.1	0.3	0.5	0.7	0.8
Z*=					
0	0	0	0	0	-.002
.100	0	-.004	-.001	0	.006
.200	0	-.008	-.004	-.004	.010
.300	-.004	-.010	-.008	-.008	.018
.400	-.006	-.013	-.006	-.008	.018
.500	-.006	-.017	-.006	-.006	.024
.600	-.012	-.024	-.008		
.700	-.014				

SPANWISE TURBULENCE LEVELS; STATION 4

R*=	0.1	0.3	0.5	0.7	0.8
Z*=					
0	.047	.012	.012	.030	.048
.100	.040	.011	.012	.030	.050
.200	.036	.011	.013	.026	.054
.300	.039	.011	.015	.028	.058
.400	.036	.012	.016	.029	.057
.500	.041	.015	.022	.030	.044
.600	.043	.021	.028		
.700	.045				

TURBULENT FLOW UV CROSS CORRELATIONS; STATION 1

R*=	0.1	0.3	0.5	0.7	0.9
Z*=					
0	-.0007	-.0000	-.0000	.0000	.0013
.100	-.0009	-.0000	.0000	.0000	.0013
.200	-.0010	-.0000	.0000	.0000	.0012
.300	-.0011	.0000	.0000	.0000	.0012
.400	-.0011	.0000	.0000	.0000	.0011
.500	-.0011	.0000	.0000	-.0000	.0012
.600	-.0009	.0001	.0001	0	.0013
.700	-.0006	.0001	.0001	-.0003	.0009
.800	-.0004	-.0002	.0002	-.0002	-.0002
.900	-.0003	-.0001	.0003	-.0003	-.0008
.925	-.0002	.0001	.0010	.0003	.0012
.950	-.0001	.0007	.0013	-.0010	.0023

TURBULENT FLOW UV CROSS CORRELATIONS; STATION 2

R*=	0.1	0.3	0.5	0.7	0.9
Z*=					
0	-.0018	-.0001	-.0000	-.0000	.0006
.100	-.0019	-.0000	-.0000	-.0000	.0006
.200	-.0022	-.0000	-.0000	-.0000	.0007
.300	-.0024	-.0000	-.0000	-.0000	.0007
.400	-.0023	-.0000	-.0000	-.0000	.0008
.500	-.0020	-.0000	-.0000	0	.0008
.600	-.0020	.0000	-.0002	.0000	.0006
.700	-.0018	-.0002	-.0004	0	.0004
.800	-.0018	-.0001	-.0003	-.0002	.0003
.900	-.0011	-.0005	-.0001	-.0006	.0003
.925	-.0010	0	0	-.0001	.0004
.950	-.0006	.0009	.0006	.0006	.0013

TURBULENT FLOW UV CROSS CORRELATIONS; STATION 3

R*=	0.1	0.3	0.5	0.7	0.9
Z*=					
0	-.0023	.0000	-.0000	.0000	.0007
.100	-.0026	.0000	-.0000	.0000	.0007
.200	-.0025	.0000	.0000	.0000	.0007
.300	-.0022	.0007	-.0000	.0000	.0009
.400	-.0024	0	0	.0001	.0010
.500	-.0023	.0000	-.0001	.0001	.0008
.600	-.0024	-.0002	-.0005	0	.0006
.700	-.0025	-.0003	-.0007	-.0001	.0004
.800	-.0020	-.0004	-.0007	-.0004	.0003
.900	-.0018	.0001	-.0002	-.0016	.0019
.925	-.0015	-.0005	-.0005	.0018	.0027
.950	-.0005	.0034	.0016	.0003	-.0002

TURBULENT FLOW UV CROSS CORRELATIONS; STATION 4

R*=	0.1	0.3	0.5	0.7	0.9
Z*=					
0	-.0012	-.0000	-.0000	.0005	.0019
.100	-.0011	-.0000	-.0000	.0004	.0019
.200	-.0012	-.0000	-.0000	.0005	.0019
.300	-.0009	-.0000	-.0000	.0005	.0018
.400	-.0007	-.0000	-.0000	.0004	.0018
.500	-.0006	-.0000	-.0000	.0005	.0017
.600	-.0010	.0000	.0000	.0005	.0014
.700	-.0009	.0002	-.0001	.0001	.0011
.800	-.0010	.0002	0	.0001	.0011
.900	-.0007	.0005	.0003	.0006	.0017
.925	-.0004	.0006	.0008	.0006	.0020
.950	0	.0013	.0015	-.0075	.0021

TURBULENT FLOW UV CROSS CORRELATIONS; STATION 5

R*=	0.1	0.3	0.5	0.7	0.9
Z*=					
0	-.0004	-.0001	0	.0015	.0022
.100	-.0004	-.0000	-.0000	.0015	.0022
.200	-.0004	-.0000	-.0000	.0018	.0014
.300	-.0003	-.0000	.0000	.0017	.0010
.400	-.0002	-.0001	.0000	.0015	.0010
.500	-.0004	.0001	.0002	.0005	.0011
.600	-.0004	.0001	.0003	.0007	.0010
.700	-.0004	.0004	.0004	.0005	.0012
.800	.0002	.0007	.0013	.0011	.0016
.900	-.0017	.0019	.0016	.0021	.0006
.925	.0021	.0031	.0021	.0025	.0013
.950	.0012	.0010	.0006	.0006	-.0009

TURBULENT FLOW STREAMWISE TURBULENCE LEVELS; STATION 1

R*=	0.1	0.3	0.5	0.7	0.9
Z*=					
0	.056	.009	.008	.011	.054
.100	.057	.009	.008	.011	.057
.200	.063	.009	.008	.011	.057
.300	.062	.009	.008	.011	.057
.400	.058	.010	.010	.012	.057
.500	.059	.015	.018	.012	.058
.600	.058	.029	.039	.020	.058
.700	.058	.057	.056	.039	.058
.800	.054	.069	.067	.062	.061
.900	.059	.080	.085	.082	.066
.925	.066	.092	.101	.098	.107
.950	.071	.120	.120	.108	.132

TURBULENT FLOW STREAMWISE TURBULENCE LEVELS; STATION 2

R*=	0.1	0.3	0.5	0.7	0.9
Z*=					
0	.072	.010	.007	.010	.053
.100	.074	.011	.007	.010	.054
.200	.078	.010	.008	.009	.056
.300	.078	.010	.008	.009	.057
.400	.078	.010	.009	.012	.057
.500	.076	.011	.016	.018	.057
.600	.073	.024	.038	.035	.054
.700	.074	.045	.053	.052	.052
.800	.076	.071	.064	.066	.062
.900	.073	.081	.076	.085	.076
.925	.073	.083	.086	.091	.092
.950	.088	.090	.092	.098	.102

TURBULENT FLOW STREAMWISE TURBULENCE LEVELS; STATION 3

R*=	0.1	0.3	0.5	0.7	0.9
Z*=					
0	.073	.010	.010	.013	.057
.100	.074	.010	.010	.014	.058
.200	.073	.013	.010	.015	.058
.300	.072	.012	.012	.017	.063
.400	.074	.012	.015	.020	.063
.500	.073	.022	.037	.030	.061
.600	.074	.048	.054	.048	.057
.700	.077	.060	.066	.056	.061
.800	.074	.064	.074	.074	.066
.900	.081	.076	.081	.091	.112
.925	.085	.088	.095	.100	.140
.950	.136	.152	.140	.112	.088

TURBULENT FLOW STREAMWISE TURBULENCE LEVELS; STATION 4

R*=	0.1	0.3	0.5	0.7	0.9
Z*=					
0	.071	.010	.009	.037	.069
.100	.071	.010	.008	.037	.069
.200	.069	.010	.008	.037	.074
.300	.064	.009	.009	.038	.076
.400	.059	.010	.011	.037	.074
.500	.066	.012	.020	.039	.068
.600	.071	.021	.037	.045	.061
.700	.069	.038	.052	.053	.056
.800	.069	.050	.059	.063	.057
.900	.068	.062	.068	.077	.078
.925	.069	.072	.076	.083	.085
.950	.071	.087	.087	.095	.090

TURBULENT FLOW STREAMWISE TURBULENCE LEVELS; STATION 5

R*=	0.1	0.3	0.5	0.7	0.9
Z*=					
0	.059	.018	.010	.057	.076
.100	.059	.012	.010	.062	.073
.200	.058	.013	.010	.064	.068
.300	.058	.013	.011	.067	.067
.400	.061	.015	.017	.060	.067
.500	.060	.020	.033	.051	.064
.600	.063	.030	.049	.047	.056
.700	.062	.042	.057	.053	.055
.800	.072	.056	.079	.069	.071
.900	.092	.099	.092	.098	.073
.925	.114	.116	.116	.108	.104
.950	.156	.156	.150	.152	.132

TURBULENT FLOW GAPWISE TURBULENCE LEVELS; STATION 1

R*=	0.1	0.3	0.5	0.7	.0.9
Z*=					
0	.040	.015	.012	.014	.053
.100	.044	.014	.011	.015	.050
.200	.040	.014	.011	.015	.045
.300	.043	.016	.012	.016	.048
.400	.043	.016	.013	.017	.050
.500	.041	.016	.020	.018	.050
.600	.047	.024	.028	.025	.051
.700	.055	.039	.048	.048	.044
.800	.062	.052	.054	.058	.061
.900	.062	.064	.057	.059	.052
.925	.062	.072	.066	.066	.055
.950	.062	.050	.049	.043	.057

TURBULENT FLOW GAPWISE TURBULENCE LEVELS; STATION 2

R*=	0.1	0.3	0.5	0.7	0.9
Z*=					
0	.048	.017	.011	.012	.033
.100	.049	.015	.011	.013	.034
.200	.056	.014	.011	.013	.037
.300	.056	.014	.011	.013	.035
.400	.056	.014	.012	.014	.037
.500	.051	.015	.014	.016	.036
.600	.053	.018	.030	.026	.034
.700	.049	.039	.043	.038	.040
.800	.053	.043	.054	.051	.047
.900	.052	.056	.058	.052	.055
.925	.052	.067	.051	.051	.047
.950	.041	.051	.051	.055	.050

TURBULENT FLOW GAPWISE TURBULENCE LEVELS; STATION 3

R*=	0.1	0.3	0.5	0.7	0.9
Z*=					
0	.059	.012	.015	.016	.035
.100	.060	.013	.016	.016	.033
.200	.059	.012	.011	.018	.037
.300	.056	.014	.010	.018	.039
.400	.044	.016	.017	.019	.040
.500	.056	.021	.025	.025	.037
.600	.056	.040	.048	.039	.039
.700	.060	.049	.062	.047	.048
.800	.052	.055	.061	.058	.055
.900	.046	.049	.073	.056	.073
.925	.077	.063	.067	.080	.069
.950	.059	.045	.069	.047	.064

TURBULENT FLOW GAPWISE TURBULENCE LEVELS; STATION 4

R*=	0.1	0.3	0.5	0.7	0.9
Z*=					
0	.043	.014	.013	.028	.047
.100	.042	.013	.013	.030	.046
.200	.042	.012	.013	.031	.045
.300	.046	.014	.013	.030	.038
.400	.036	.014	.015	.030	.047
.500	.030	.015	.023	.032	.049
.600	.036	.020	.030	.034	.045
.700	.042	.034	.041	.052	.043
.800	.042	.041	.051	.051	.050
.900	.045	.050	.053	.060	.056
.925	.047	.053	.056	.057	.056
.950	.054	.053	.053	.062	.047

TURBULENT FLOW GAPWISE TURBULENCE LEVELS; STATION 5

R*=	0.1	0.3	0.5	0.7	0.9
Z*=					
0	.036	.015	.012	.046	.057
.100	.034	.017	.011	.042	.058
.200	.033	.016	.012	.045	.053
.300	.038	.017	.013	.045	.055
.400	.034	.019	.017	.044	.056
.500	.042	.022	.027	.043	.053
.600	.037	.024	.040	.041	.052
.700	.039	.034	.049	.046	.052
.800	.044	.039	.063	.059	.061
.900	.049	.058	.062	.069	.061
.925	.021	.061	.048	.069	.038
.950	.053	.065	.067	.071	.059

TABLE III - S-DUCT OF SQUARE CROSS-SECTION. TURBULENT FLOW :

REYNOLDS NUMBER 40 000. WALL PRESSURE MEASUREMENTS

Streamwise station X_H	Radial location r*	Spanwise location z*	Pressure coefficient $C_p = \frac{P-P_{ref}}{\frac{1}{2}\rho V_b^2}$
-1.0	0.0	0.0	0.000 (P_{ref})
	0.5	1.0	-0.027
	1.0	0.0	-0.060
1.1	0.0	0.0	0.043
	0.0	0.75	0.037
	0.1	1.0	0.026
	0.3	1.0	-0.060
	0.5	1.0	-0.102
	0.7	1.0	-0.162
	0.9	1.0	-0.184
	1.0	0.75	-0.223
	1.0	0.0	-0.230
2.2	0.0	0.0	0.035
	0.1	1.0	0.011
	0.3	1.0	-0.062
	0.5	1.0	-0.102
	0.7	1.0	-0.137
	0.9	1.0	-0.184
	1.0	0.0	-0.215
3.3	0.0	0.0	-0.290
	0.0	0.75	-0.285
	0.1	1.0	-0.219
	0.3	1.0	-0.209
	0.5	1.0	-0.162
	0.7	1.0	-0.141
	0.9	1.0	-0.080
	1.0	0.75	-0.065
	1.0	0.0	-0.062
4.4	0.0	0.0	-0.359
	0.1	1.0	-0.327
	0.3	1.0	-0.257
	0.5	1.0	-0.196
	0.7	1.0	-0.117
	0.9	1.0	-0.103
	1.0	0.0	-0.084
6.5	0.0	0.0	-0.235
	0.5	1.0	-0.220
	1.0	0.0	-0.210

APPENDIX 2

DEFINITION OF SYMBOLS

Roman Characters

C_p	Pressure coefficient (figure 13)
D_H	Hydraulic diameter (40 mm)
De	Dean number: $De \equiv \left[\frac{\frac{1}{2}D_H}{R_c}\right]^{\frac{1}{2}}$. Re
P	Pressure at wall
P_{ref}	Reference value of P (X_H = 0.0, r* = 0, z* = 0)
r	Radial co-ordinate direction (figure 1)
r_i	Radius of curvature of suction surface (see figure 1)
r_o	Radius of curvature of pressure surface (see figure 1)
r*	Normalised radial co-ordinate: $r^* \equiv \frac{r - r_o}{r_i - r_o}$
R_c	Mean radius of curvature: $R_c \equiv \frac{1}{2}(r_i + r_o)$
Re	Reynolds number based on V_b and X_H
U	Velocity in streamwise direction
$\tilde{u}$	R.m.s. fluctuating velocity in streamwise direction
$\overline{uv}$	Cross-correlation between $\tilde{u}$ and $\tilde{v}$ (time-averaged)
V	Velocity in radial direction
V_b	Bulk mean velocity (mass flow rate/duct area)
$\tilde{v}$	R.m.s. fluctuating velocity in radial direction
W	Velocity in spanwise direction
$\tilde{w}$	R.m.s. fluctuating velocity in spanwise direction
X_H	Distance along duct centre-line, expressed in hydraulic diameters
z	Spanwise co-ordinate direction

$z_{\frac{1}{2}}$ Duct half-width (20 mm)

z^* Normalised spanwise co-ordinate: $z^* \equiv \frac{z}{z_{\frac{1}{2}}}$ (see figure 1)

Greek Characters

θ Streamwise co-ordinate direction

Operators

$\overline{\ldots}$ Time-averaged quantity

REFERENCES

1. Rowe, M. (1970). Measurements and computations of flow in pipe bends. J. Fluid Mech., 43, part 4, 771-783.
2. Bansod, P. and Bradshaw, P. (1972). The flow in S-shaped ducts. Aeronautical quarterly, 23, part 2, 131-140.
3. Butz, L.A. (1979). Turbulent flow in S-shaped ducts. M.Sc. thesis, Purdue University.
4. Taylor, A.M.K.P., Whitelaw, J.H. and Yianneskis, M. (1981). Measurements of laminar and turbulent flow in a curved duct with thin inlet boundary layers. NASA Contractor Report 3367.
5. Melling, A. and Whitelaw, J.H. (1976). Turbulent flow in a rectangular duct. J. Fluid Mech., 78, 289.
6. Taylor, A.M.K.P., Whitelaw, J.H. and Yianneskis, M. (1981). Curved ducts with strong secondary motion: measurements of developing laminar and turbulent flow. Imperial College, Mech. Eng. Dept. Report FS/81/20. To be published in the J. Fluids Engng, A.S.M.E.
7. Scorer, R.S. (1978). Environmental aerodynamics. Ellis Horwood, Chichester.

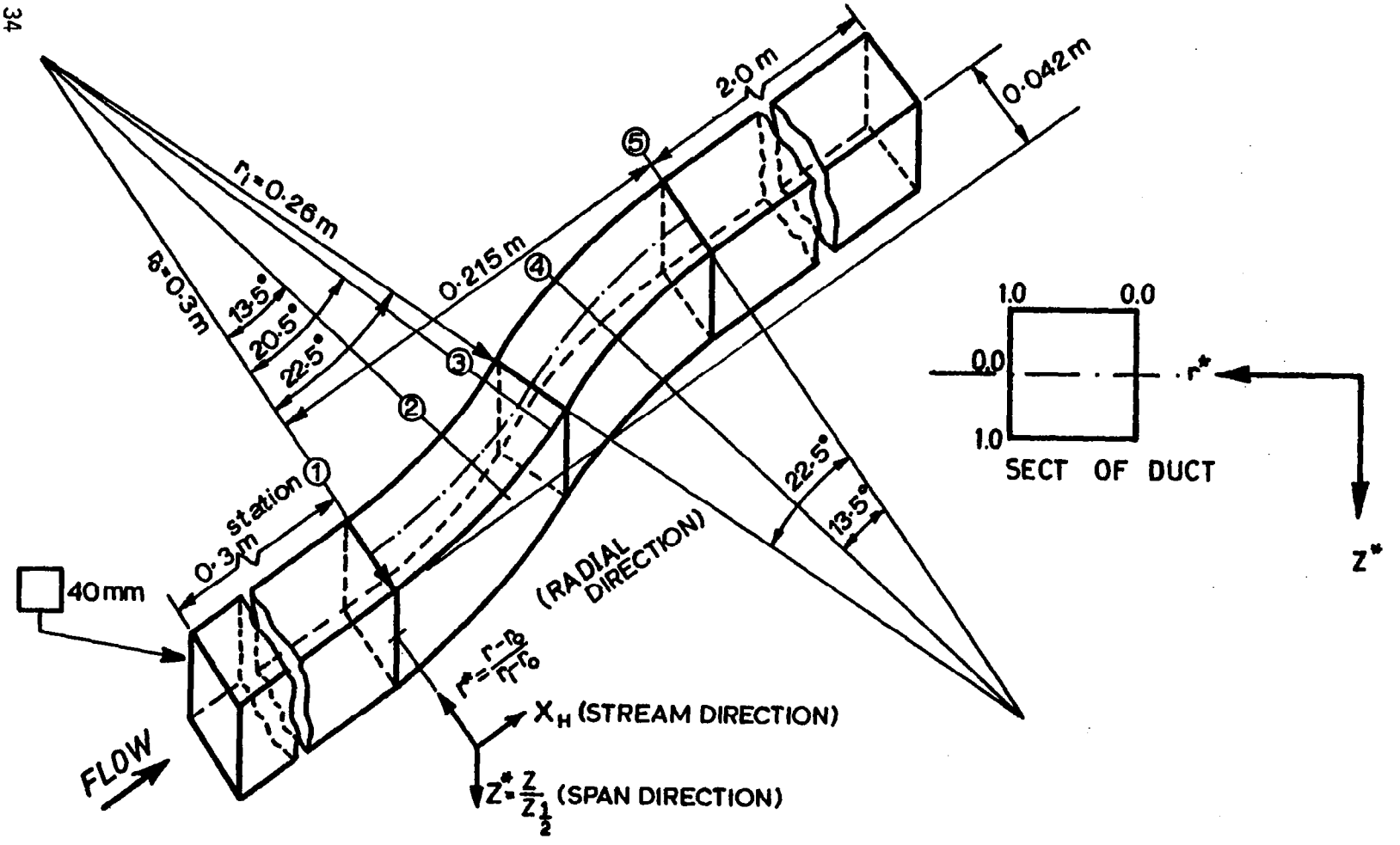

Fig. 1 Flow configuration and co-ordinate sketch

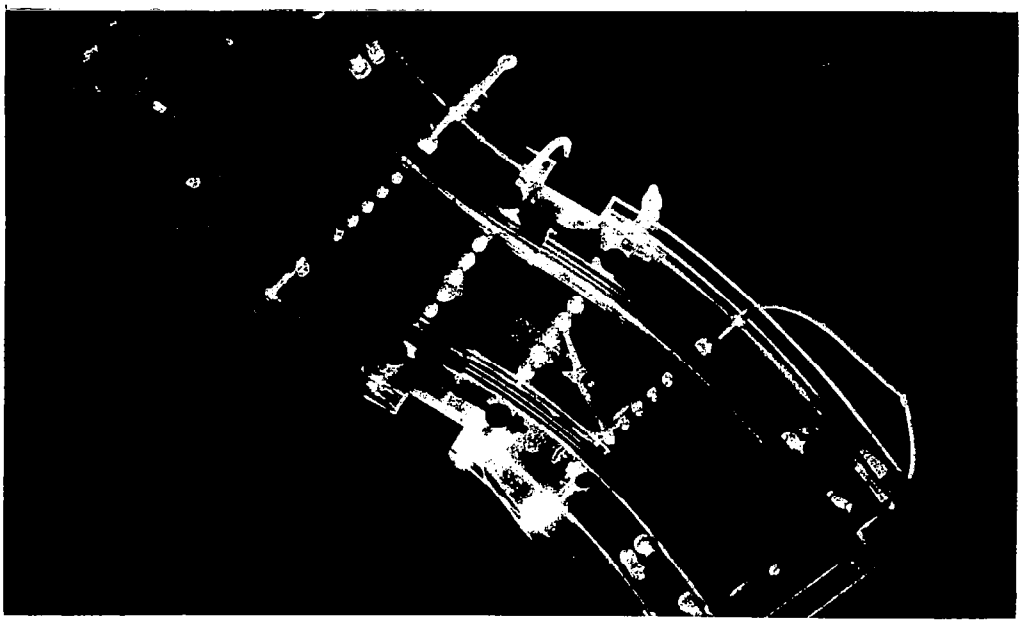

Fig. 2(i) Visualization of "core" flow through S-bend. Re = 1275. Flow direction from top left to bottom right. Wire inserted at X_H = - 1.0, r* = 0.5.

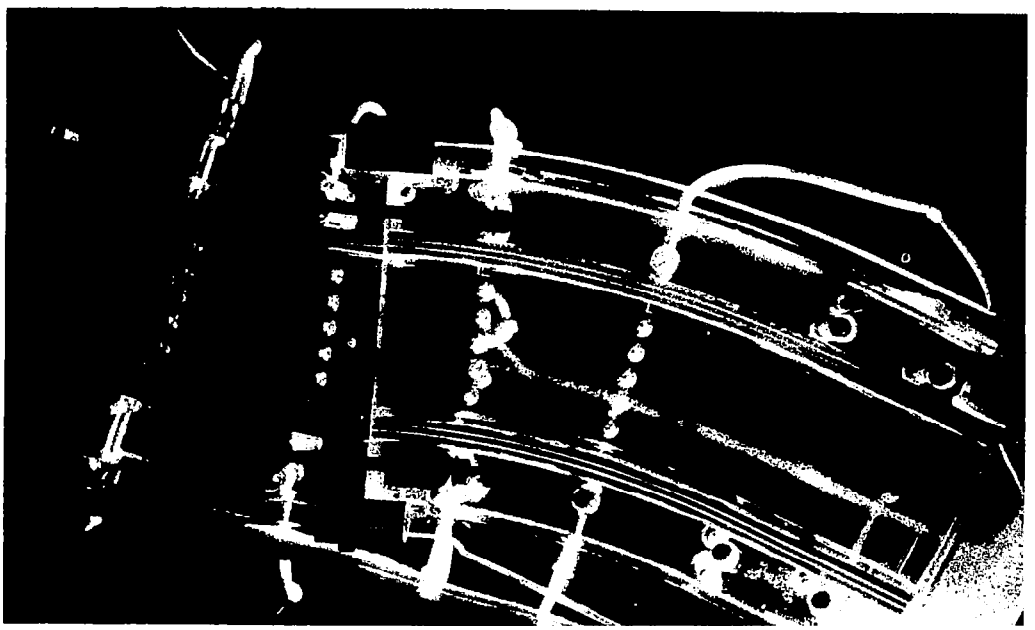

Fig. 2(ii) Visualization of secondary flow in S-bend. Re = 1275. Flow direction left to right. Wire inserted at X_H = 1.1, r* = 0.5.

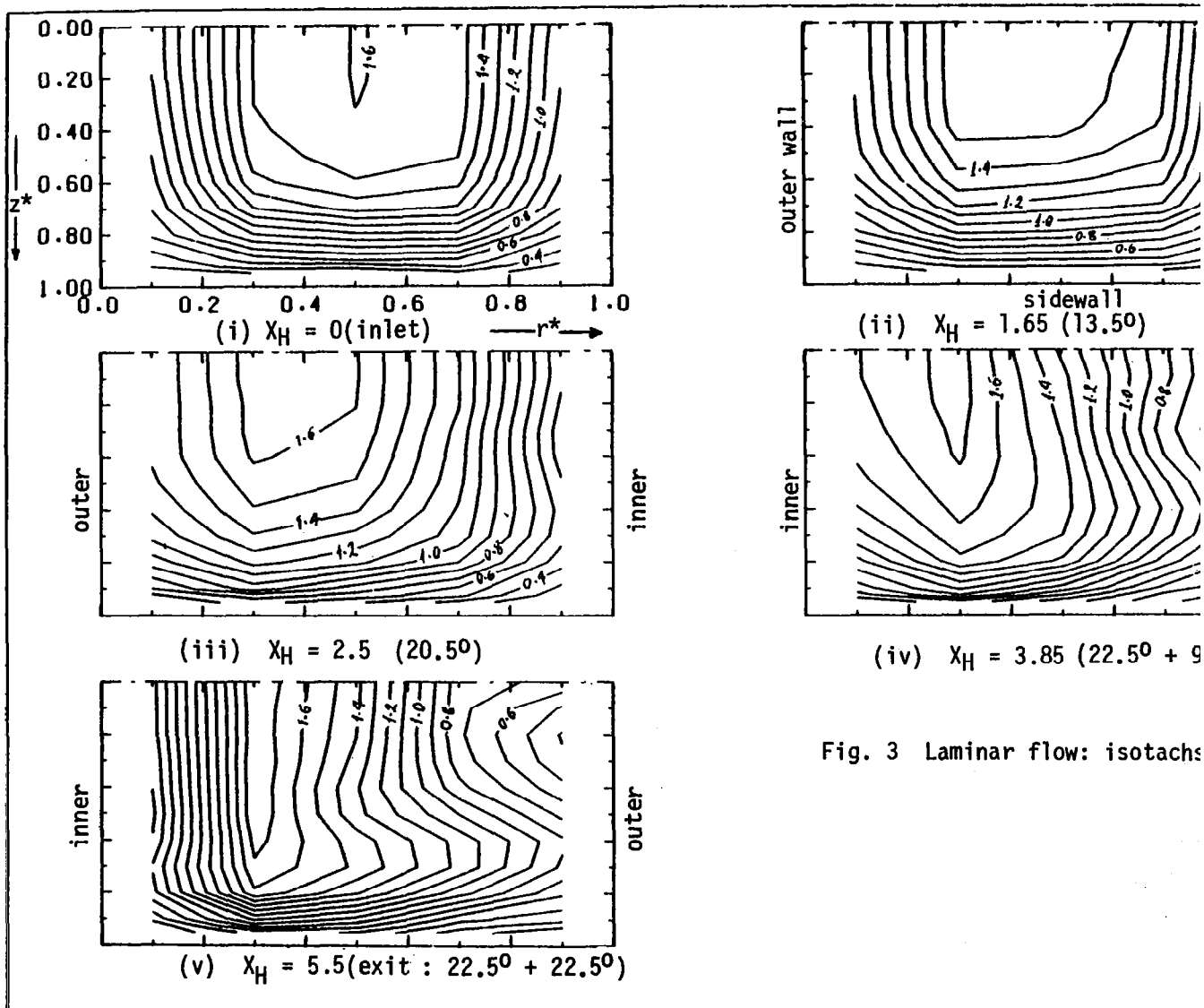

Fig. 3 Laminar flow: isotachs

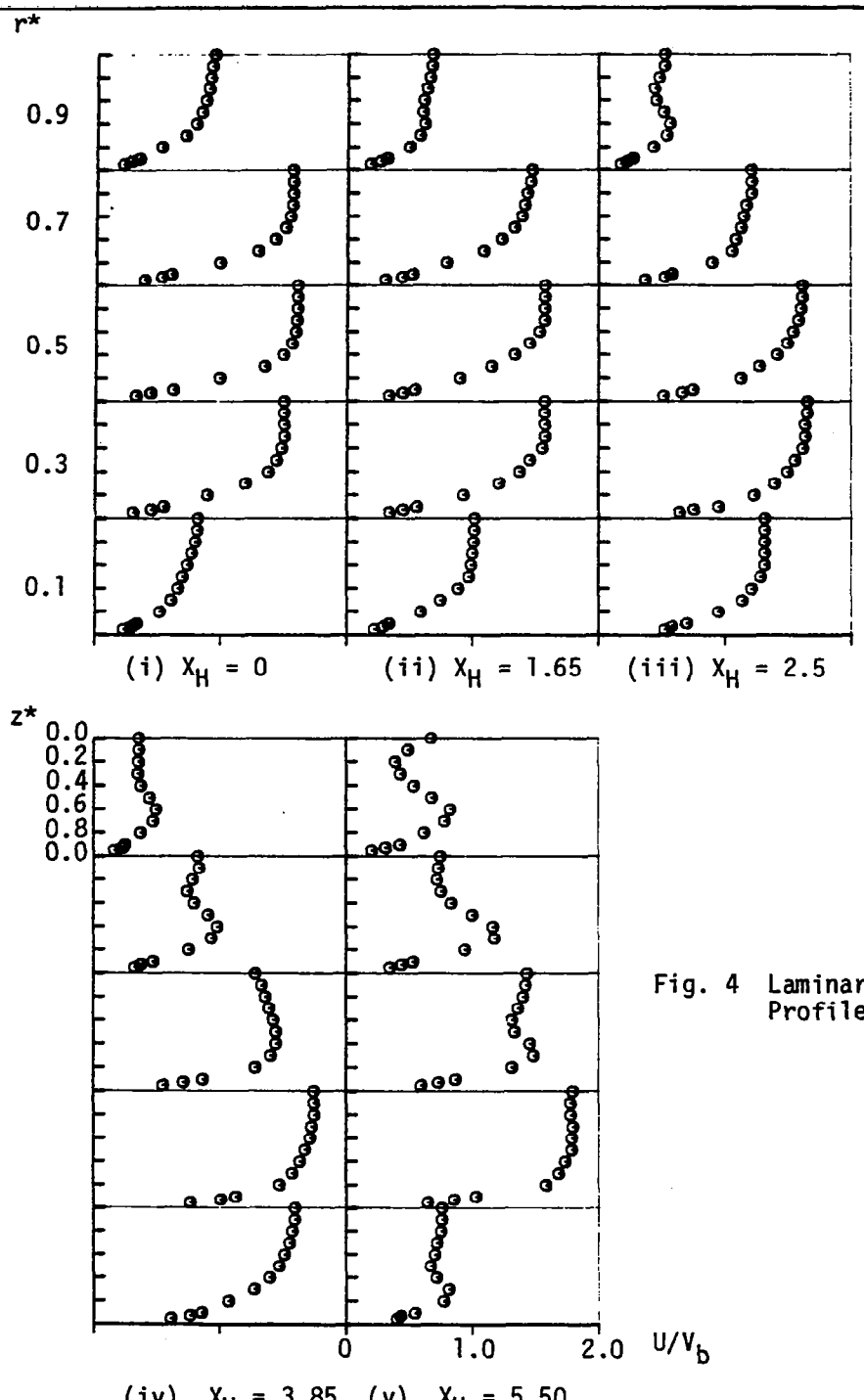

Fig. 4 Laminar flow: Profiles of U/V_b

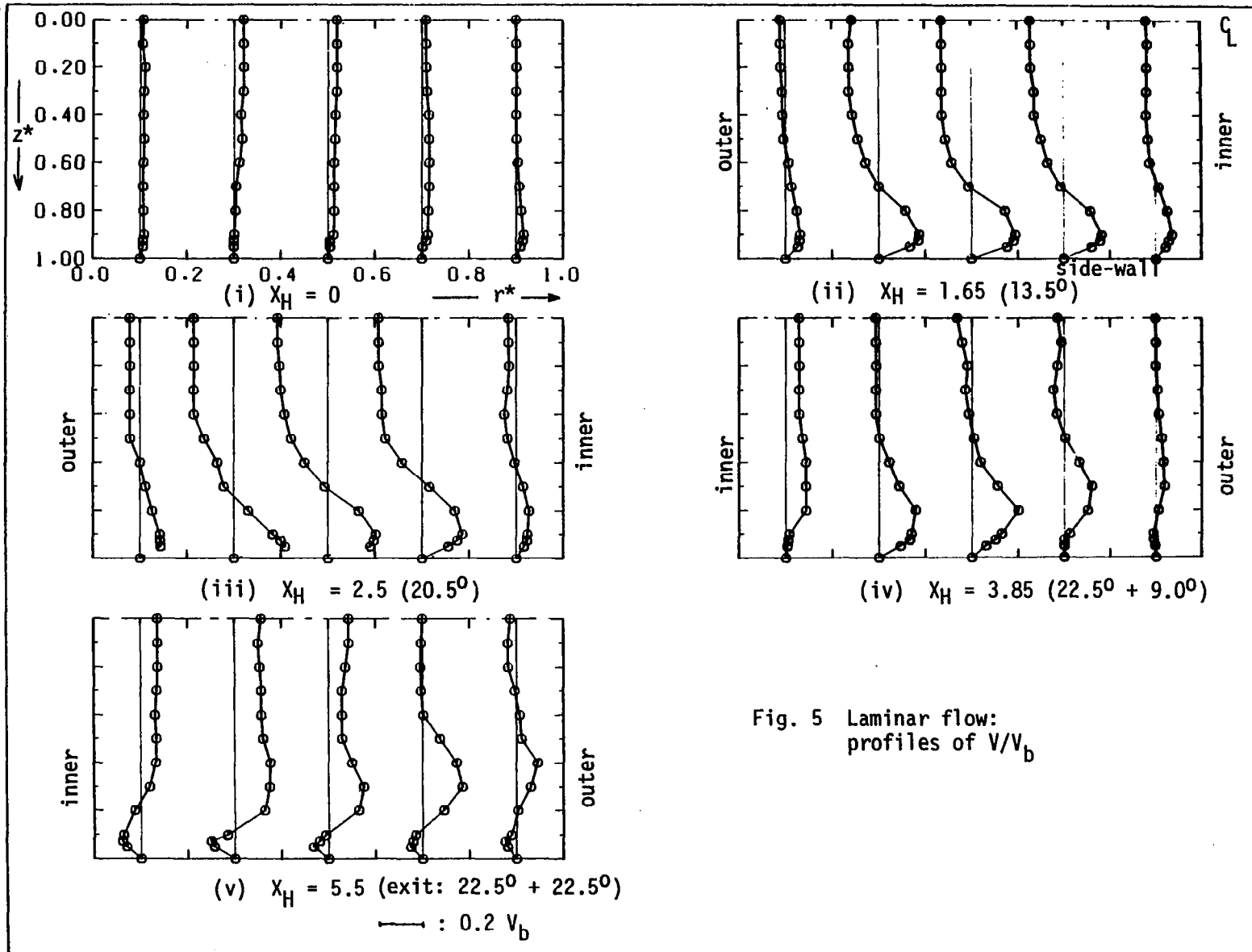

Fig. 5 Laminar flow: profiles of V/V_b

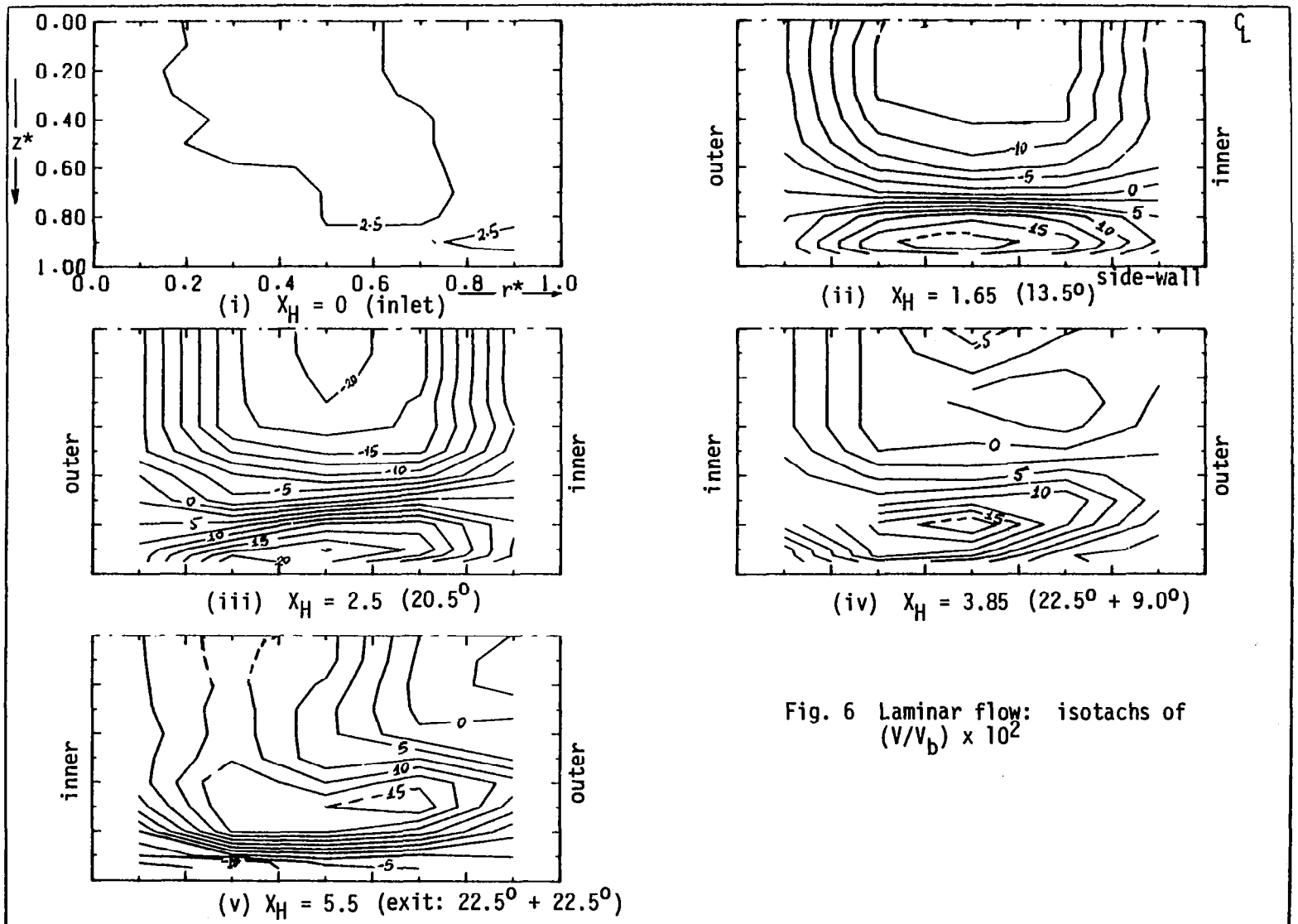

Fig. 6 Laminar flow: isotachs of $(V/V_b) \times 10^2$

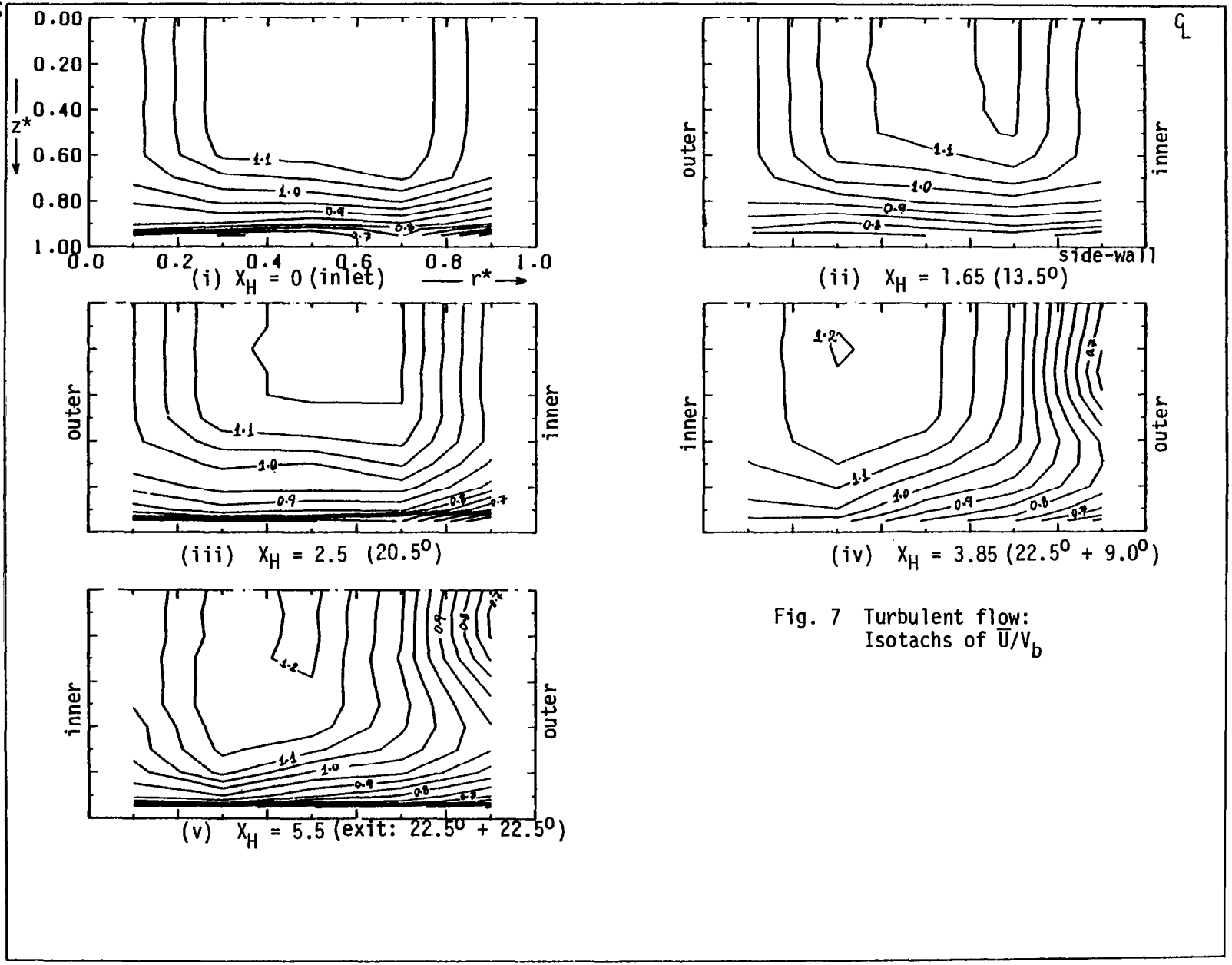

Fig. 7 Turbulent flow:
Isotachs of $\overline{U}/V_b$

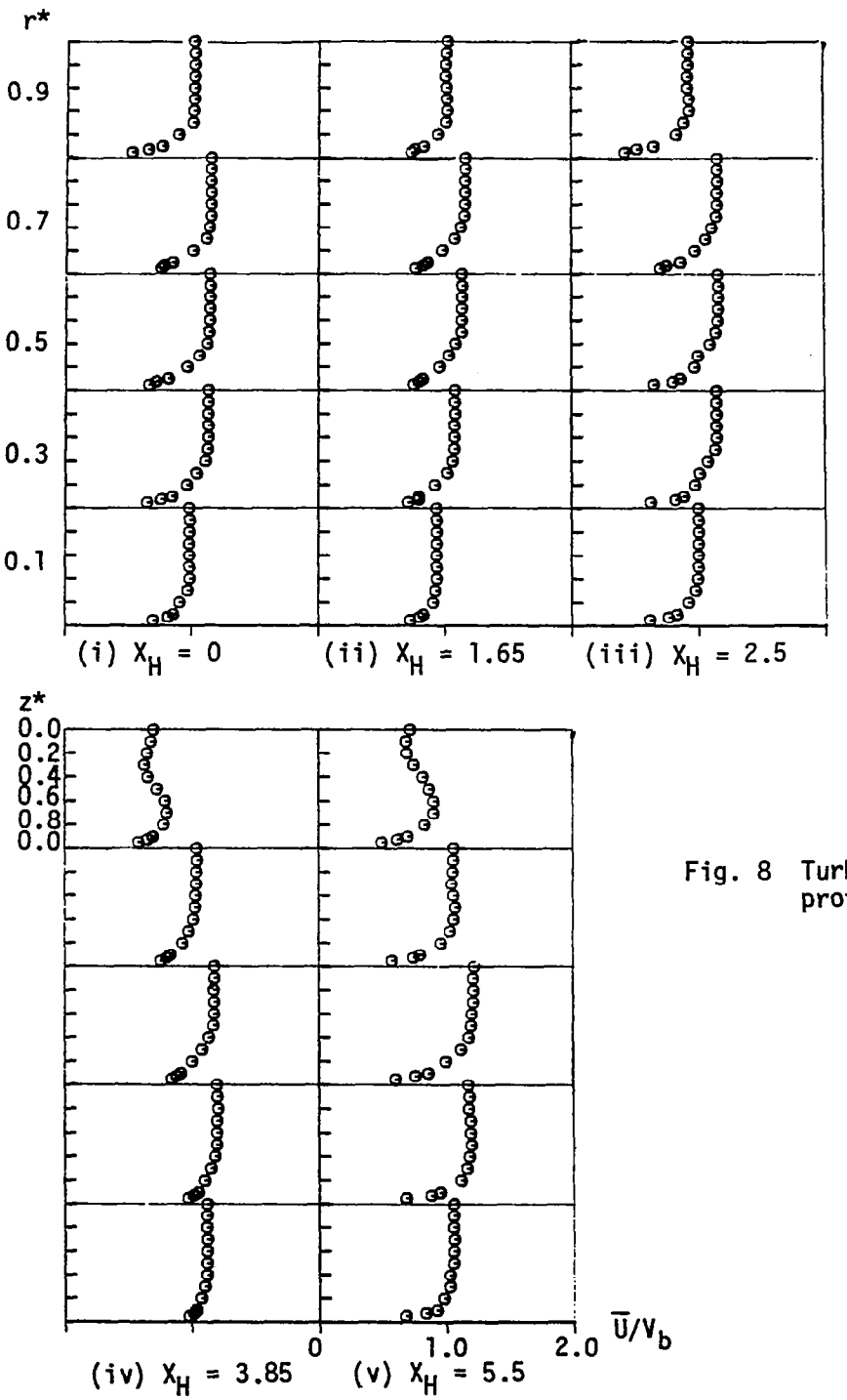

Fig. 8 Turbulent flow: profiles of $\bar{U}/V_b$

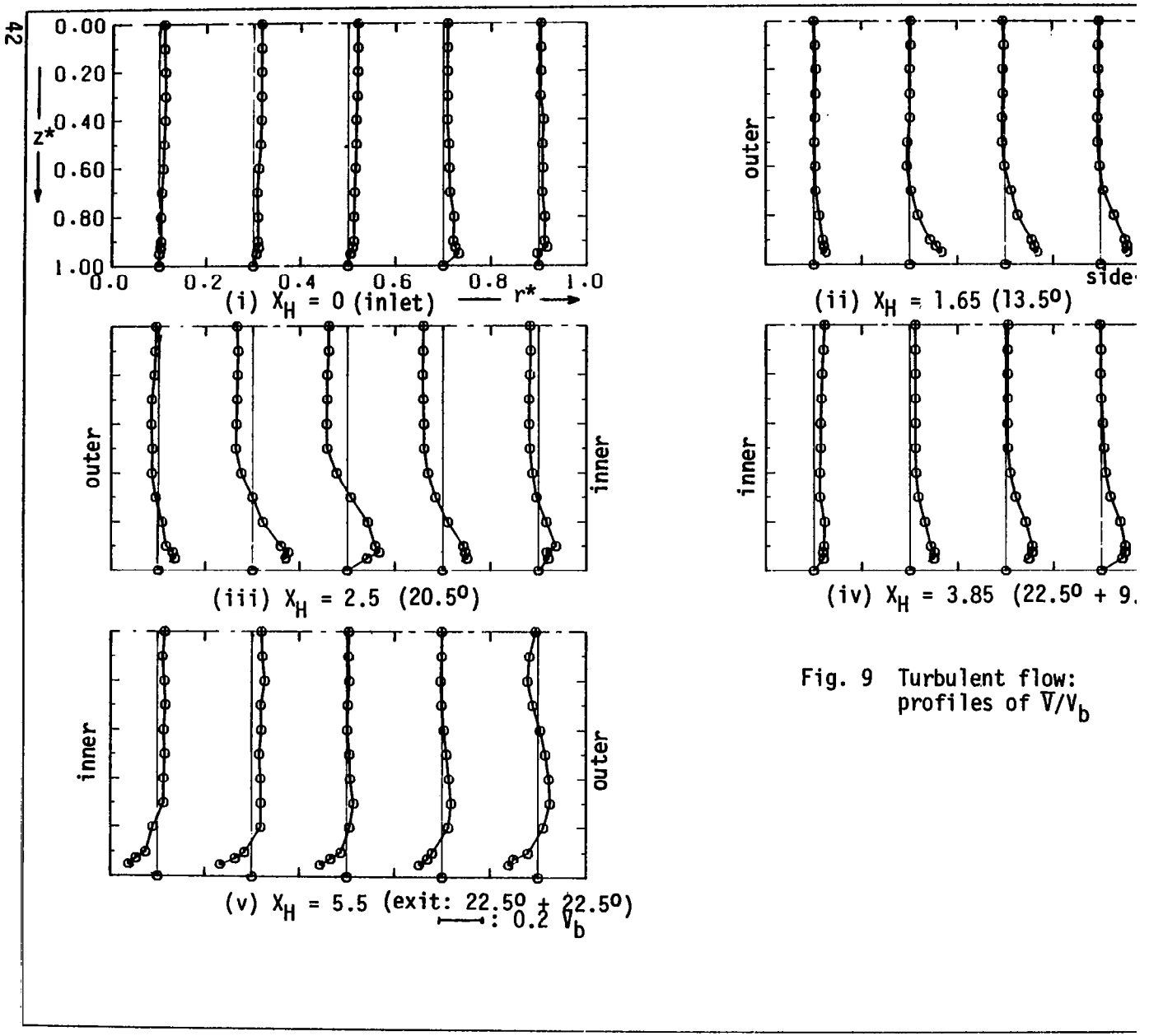

Fig. 9 Turbulent flow: profiles of $\overline{V}/V_b$

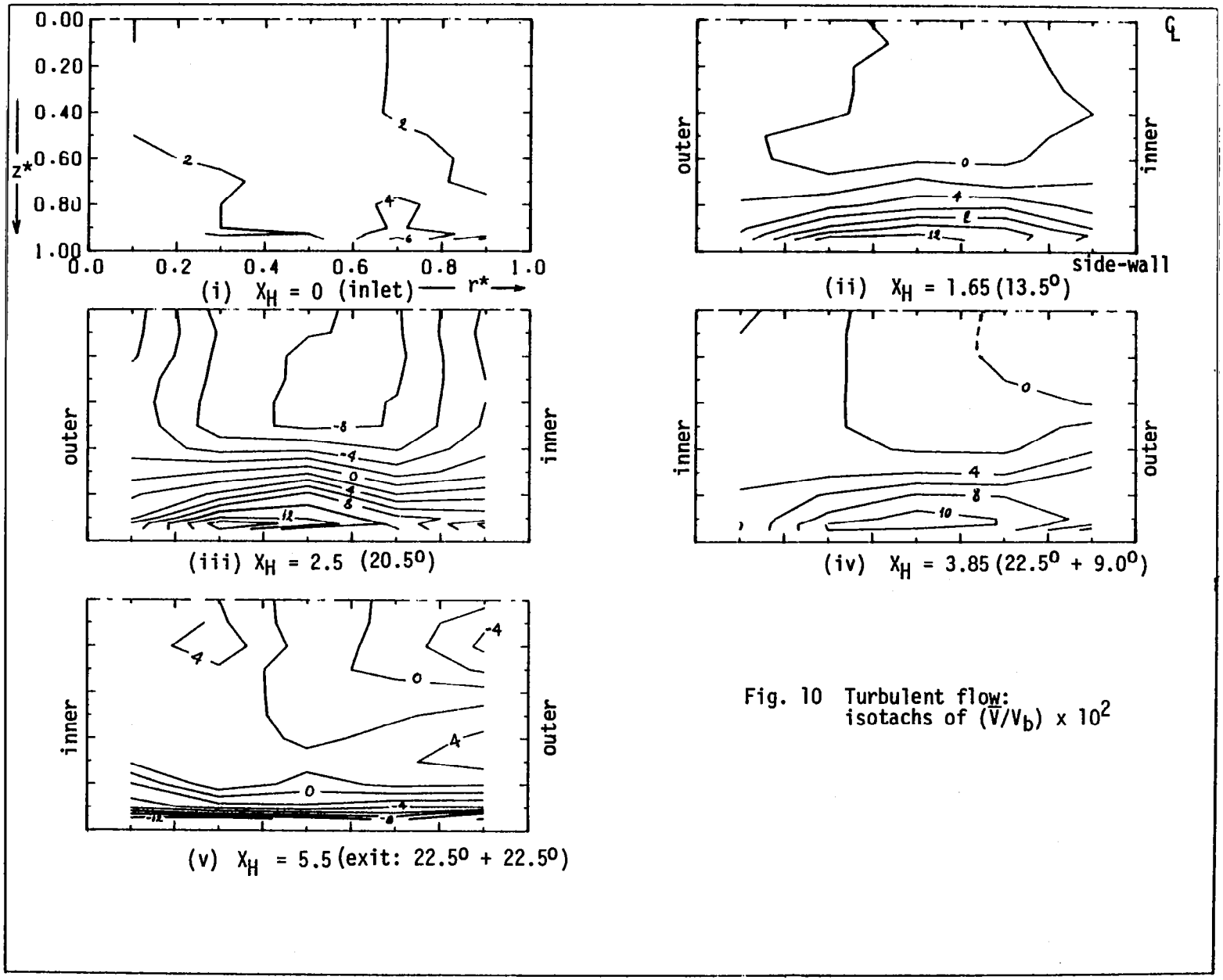

Fig. 10 Turbulent flow:
isotachs of $(\bar{V}/V_b) \times 10^2$

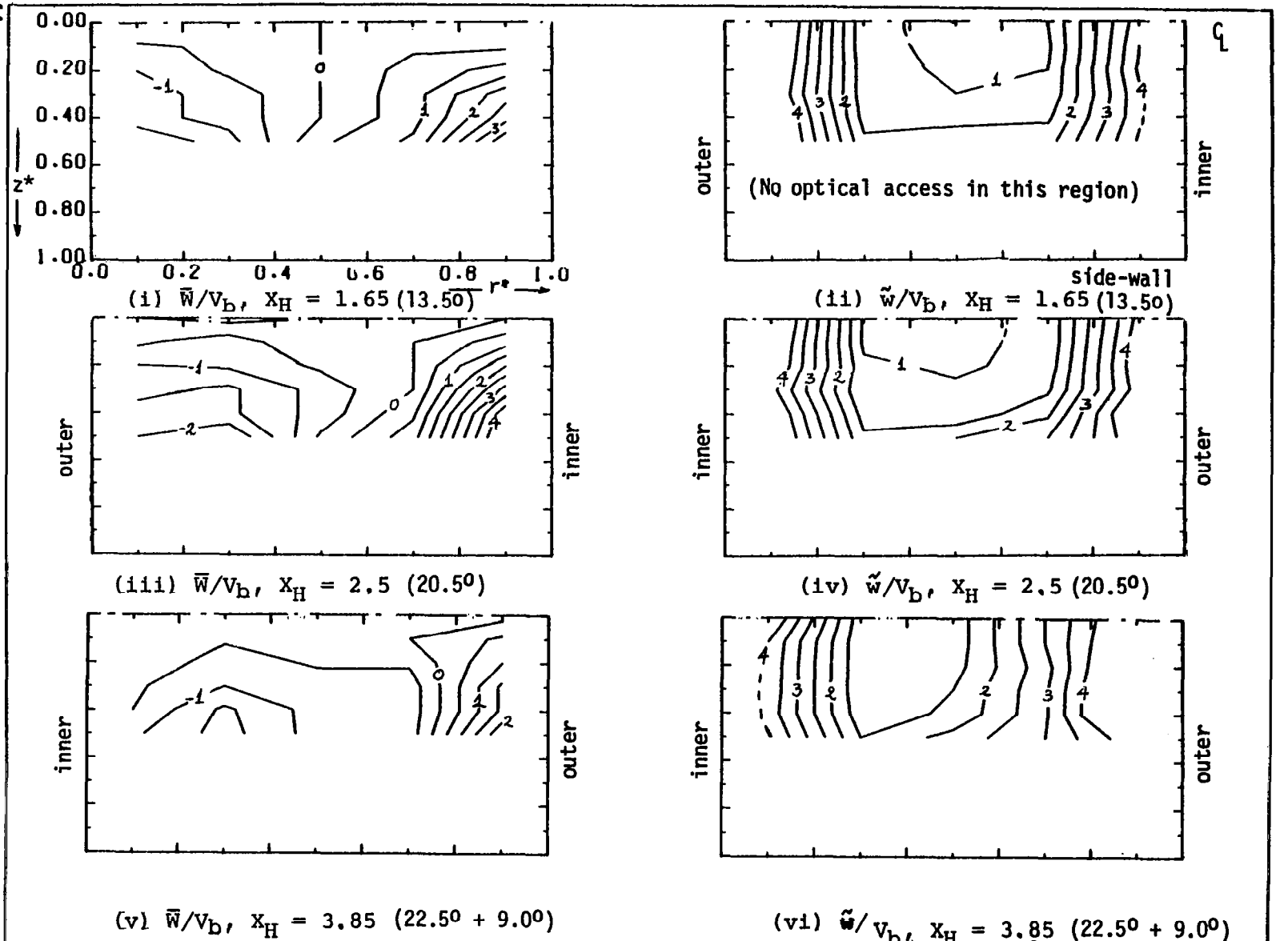

Fig. 11. Turbulent flow: Contours of $(\bar{W}/V_b) \times 10^2$ and $(\tilde{w}/V_b) \times 10^2$

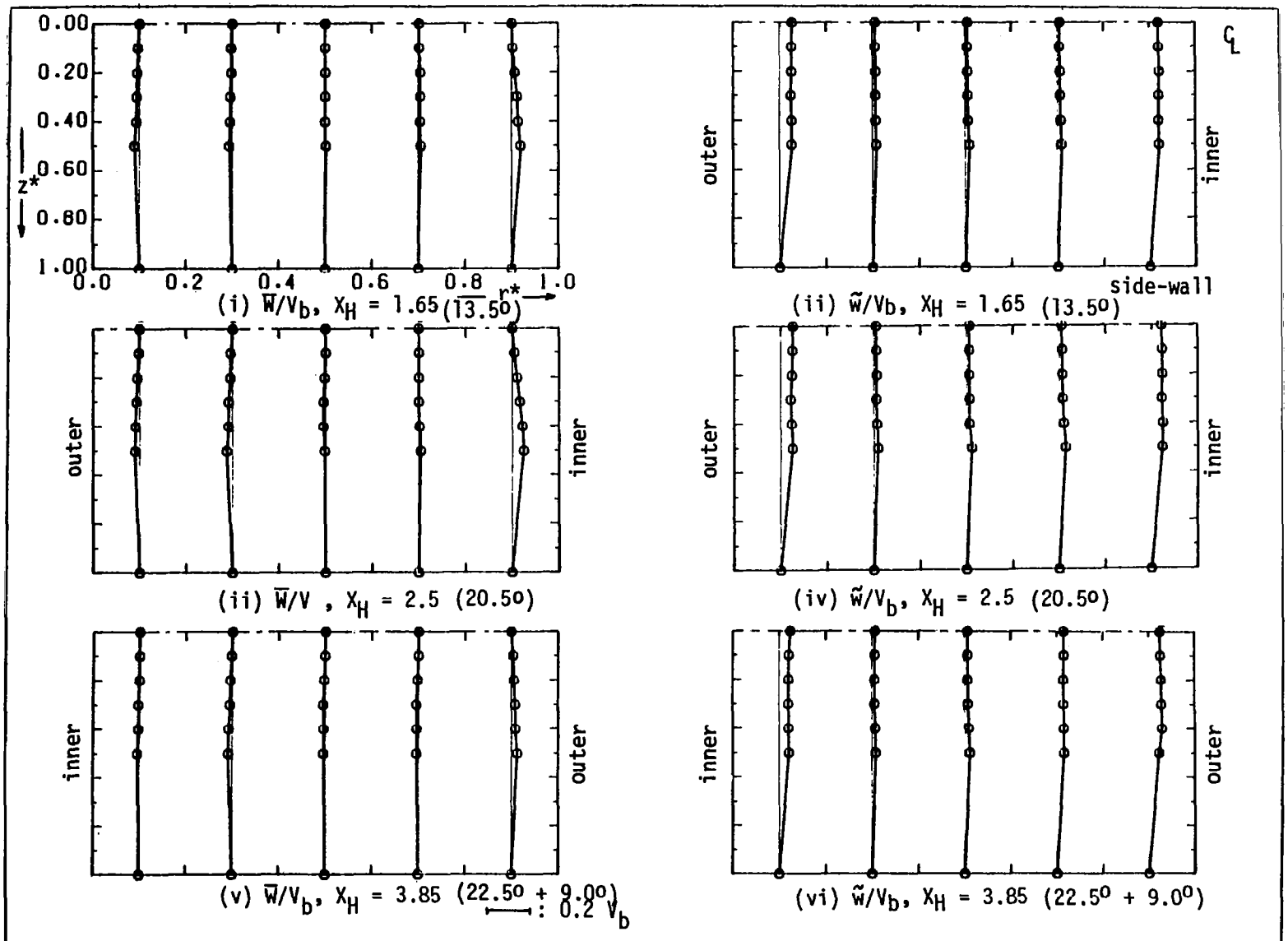

Fig. 12 Turbulent flow: profiles of $\overline{W}/V_b$ and $\tilde{w}/V_b$

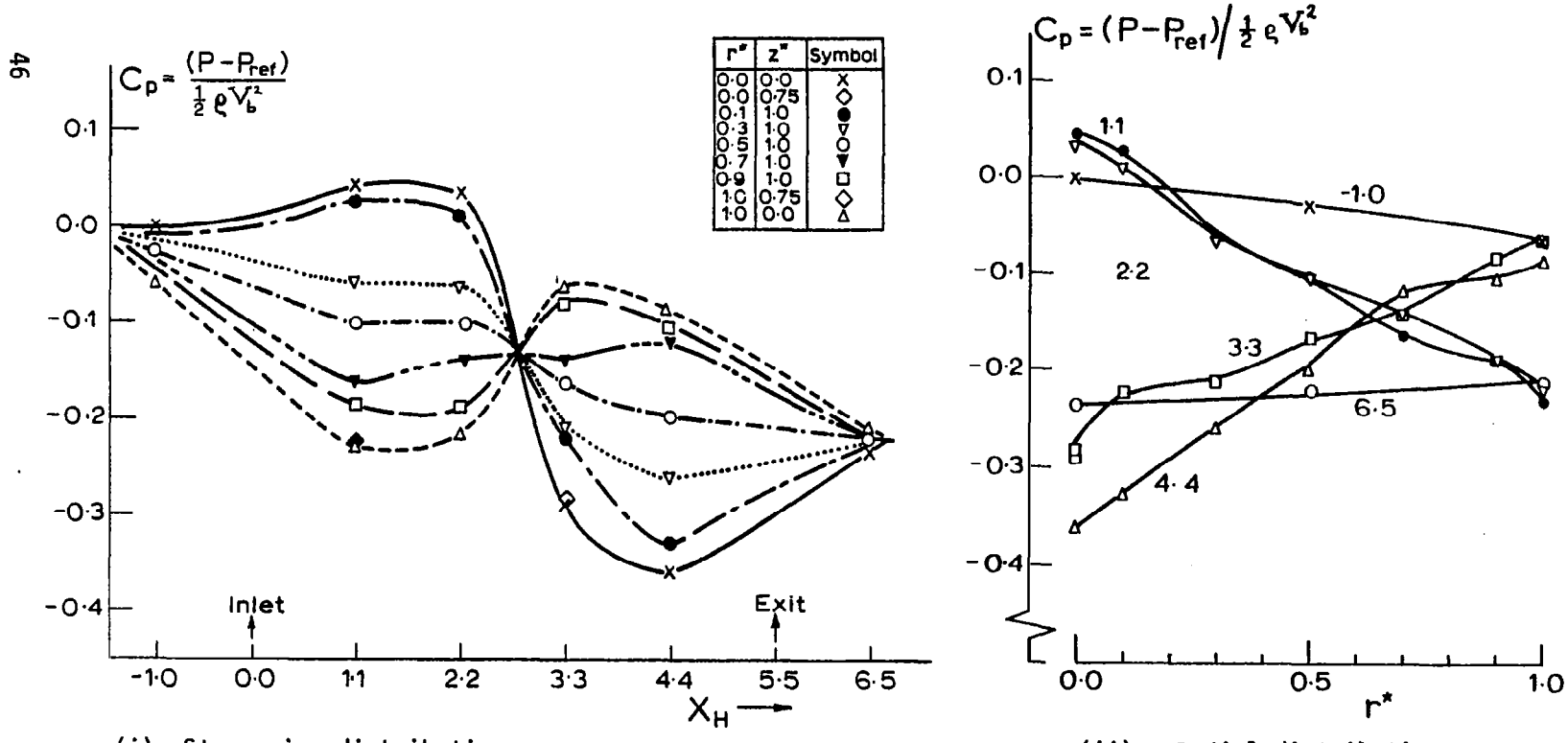

(i) Streamwise distribution

(ii) Radial distribution

Fig. 13 Turbulent flow: wall static pressure measurements

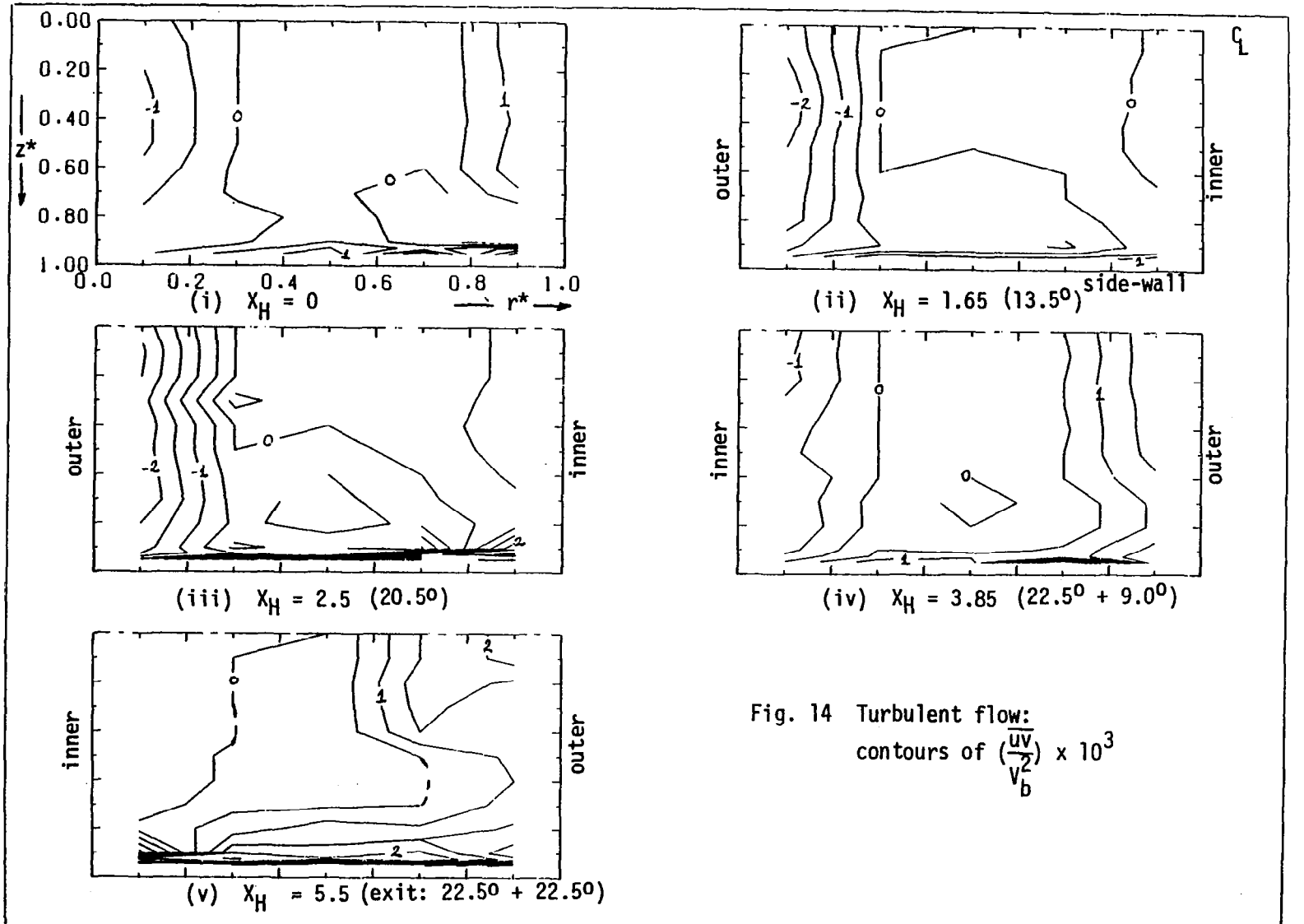

Fig. 14 Turbulent flow:
contours of $(\frac{\overline{uv}}{V_b^2}) \times 10^3$

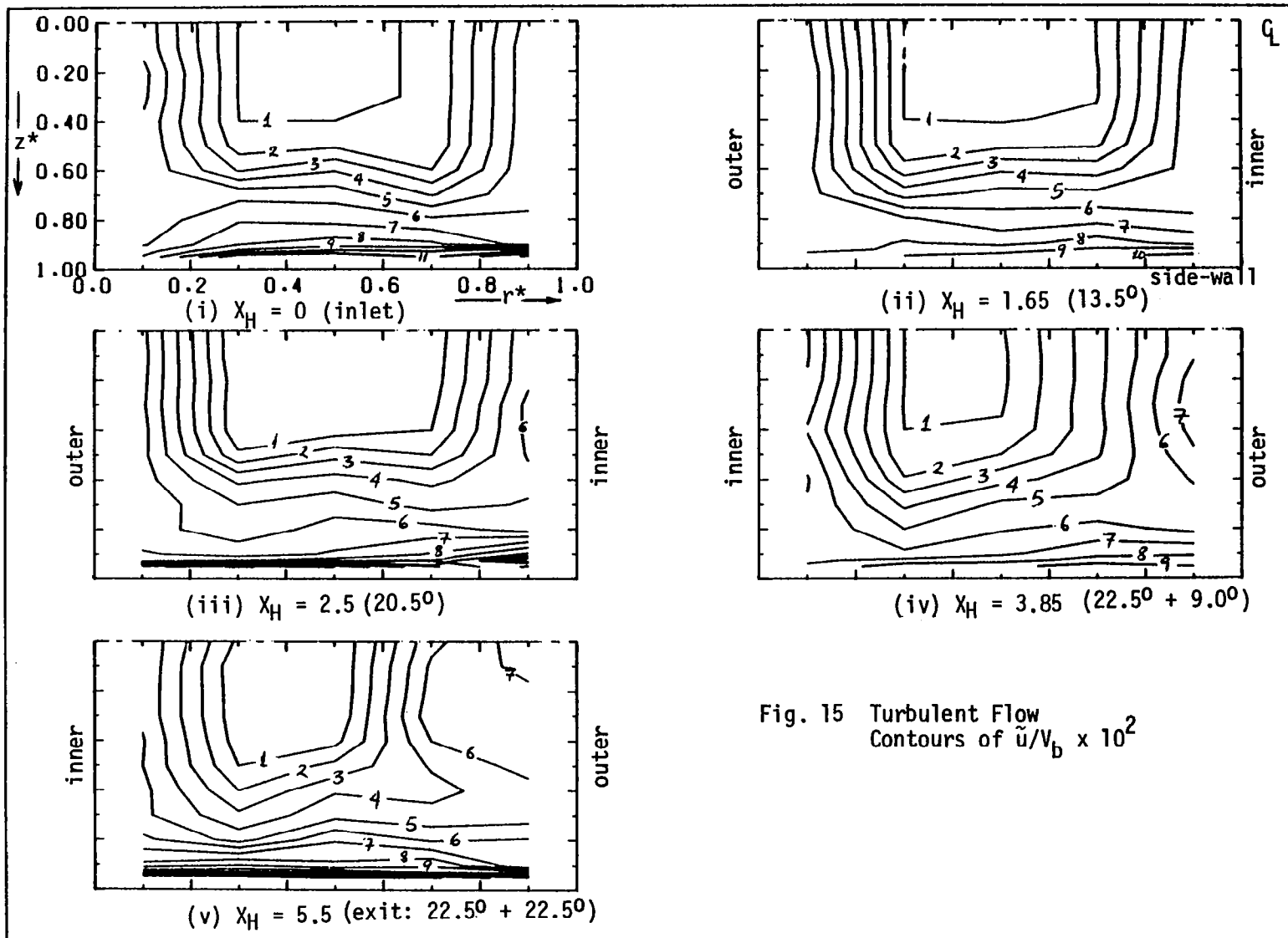

Fig. 15 Turbulent Flow
Contours of $\tilde{u}/V_b \times 10^2$

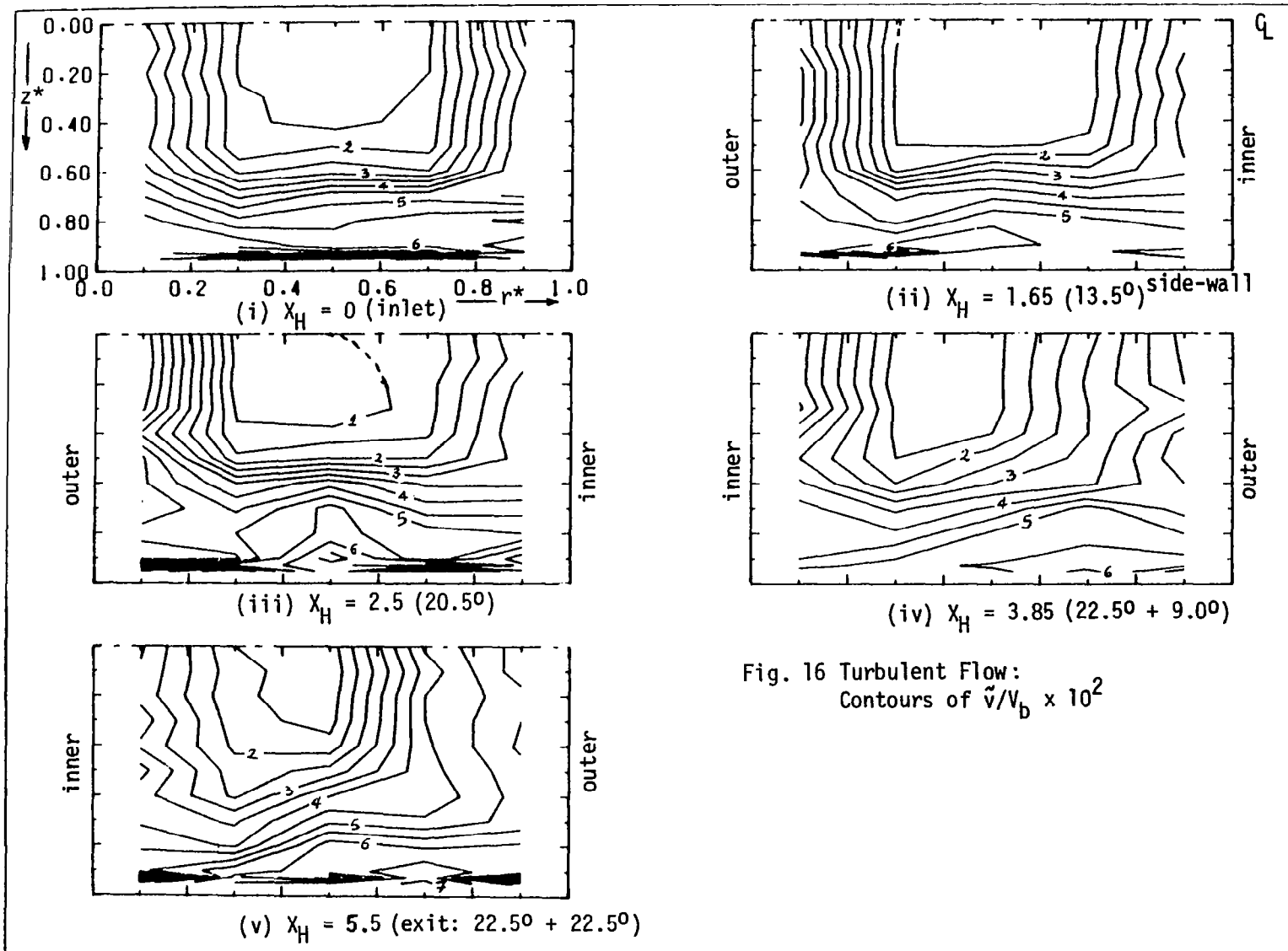

Fig. 16 Turbulent Flow:
Contours of $\tilde{v}/V_b \times 10^2$

1. Report No.	2. Government Accession No.	3. Recipient's Catalog No.
NASA CR-3550		

4. Title and Subtitle	5. Report Date
DEVELOPING FLOW IN S-SHAPED DUCTS I - SQUARE CROSS-SECTION DUCT	May 1982
	6. Performing Organization Code
7. Author(s)	8. Performing Organization Report No.
A. M. K. P. Taylor, J. H. Whitelaw, and M. Yianneskis	FS/81/22
	10. Work Unit No.
9. Performing Organization Name and Address	
Imperial College of Science and Technology Department of Mechanical Engineering Exhibition Road London SW7 2BX, England	11. Contract or Grant No. NASW-3435
	13. Type of Report and Period Covered Contractor Report
12. Sponsoring Agency Name and Address	
National Aeronautics and Space Administration Washington, D. C. 20546	14. Sponsoring Agency Code 505-32-12

15. Supplementary Notes

Final report. Project Manager, Louis A. Povinelli, Aerothermodynamics and Fuels Division, NASA Lewis Research Center, Cleveland Ohio 44135.

16. Abstract

Laser-Doppler velocimetry was used to measure the laminar and turbulent flow in an S-duct formed with two 22.5° sectors of a bend with ratio of mean radius of curvature to hydraulic diameter of 7.0. The boundary layers at the inlet to the bend were about 25% and 15% of the hydraulic diameter for the laminar and turbulent flows, respectively. Pressure-driven secondary flows develop in the first half of the S-duct and persist into the second half but are largely reversed by the exit plane as a consequence of the change in the sense of curvature. There is, however, a region near the outer wall of the second bend where the redistribution of the streamwise isotachs results in a reinforcement of the secondary flow which was established in the first half of the S-duct. The net redistribution of the streamwise isotachs is comparable to that occurring in unidirectional bends of stronger curvature. The wall pressure distribution was also measured for the turbulent flow and quantifies the expected large variations in the longitudinal pressure-gradient distributions which occur at different radial locations.

17. Key Words (Suggested by Author(s))	18. Distribution Statement
Secondary flow Laser-Doppler velocimeter Ducts - intake systems	Unclassified - unlimited STAR Category 34

19. Security Classif. (of this report)	20. Security Classif. (of this page)	21. No. of Pages	22. Price*
Unclassified	Unclassified	52	A04

* For sale by the National Technical Information Service, Springfield, Virginia 22161

NASA-Langley, 1982